An Ab Initio G3-Type/Statistical Theory Study of the Formation of Indene in Combustion Flames. II. The Pathways Originating from Reactions of Cyclic C_5 Species—Cyclopentadiene and Cyclopentadienyl Radicals

V. V. Kislov[†] and A. M. Mebel*

Department of Chemistry and Biochemistry, Florida International University, Miami, Florida 33199

Received: September 17, 2007; In Final Form: October 29, 2007

Chemically accurate ab initio Gaussian-3-type calculations of various rearrangements on the $C_{10}H_{11}$ potential energy surface have been performed to investigate the indene formation mechanism originating from the reactions of two abundant cyclic C_5 species, cyclopentadiene and cyclopentadienyl radicals. Using the accurate ab initio data, statistical theory calculations have been applied to obtain high-pressure-limit thermal rate constants within the 300−3000 K temperature range, followed by calculations of relative product yields. Totally, 12 reaction pathways leading to indene and several azulene precursors, 1,5-, 1,7-, 1,8a-, and 1,3a-dihydroazulene, have been mapped out, and the relative contributions of each pathway to the formation of reaction products have been estimated. At temperatures relevant to combustion, the indene has been found as the major reaction product (>50%) followed by 1,5-dihydroazulene (25−35%), whereas all other products demonstrate either minor or negligible yields. The results of the present study have been combined with our previous data for rearrangements of the 9-H-fulvalenyl radical on the $C_{10}H_9$ potential energy surface to draw the detailed picture of radical-promoted reaction mechanisms leading from *c*-C_5 species to the production of indene, naphthalene, azulene, and fulvalene in combustion. The suggested mechanism and computed product yields are consistent with the experimental data obtained in the low-temperature pyrolysis of cyclopentadiene, where indene and naphthalene have been found as the major reaction products.

1. Introduction

The formation of indene, the simplest among cyclopentafused polycyclic aromatic hydrocarbons (PAHs), in combustion flames and in pyrolysis of hydrocarbon fuels can be accomplished by various pathways involving a variety of abundant building blocks, such as acetylene, propargyl radical, cyclopentadiene (**CPD**) and cyclopentadienyl radicals (**CPDyl**), fulvene, benzene/phenyl, toluene/benzyl, and even naphthalene.[1−8] A number of mechanisms have been suggested based on experimental observations,[1−5] but only some of them have been investigated theoretically using ab initio and DFT methods.[6,8] According to these studies, the most significant pathways include the reaction of the benzyl radical with acetylene (1,3-butadiene flame, Granata et al.,[4]), oxidation of the naphthyl radical (*n*-butane and ethylene flames, Marinov et al.[1−3]), and the radical−molecule reaction of **CPDyl** with **CPD** (**CPD** pyrolysis, Wang et al.[6]). All suggested mechanisms require thorough investigation by theoretical methods to provide accurate information on potential energy surfaces (PES), reaction barriers, molecular parameters, and rate constants, which can then be utilized in kinetic modeling of flame combustion.

In our previous study, we carefully studied the reaction pathways relevant to the formation of an additional cyclopenta ring over the existing six-member aromatic rings of benzene/phenyl and toluene/benzyl, producing indene.[8] The most abundant small species, such as the propargyl radical (C_3H_3), methyl radical (CH_3), methylene (CH_2), and acetylene (C_2H_2), were considered as the building fragments in the formation of an extra C_5 moiety. The studied pathways included recombination of phenyl and propargyl radicals, intermolecular addition of the propargyl radical to benzene, and the HACA (hydrogen abstraction acetylene addition)-type acetylene addition to the benzyl radical. The Gaussian-3-type calculations were applied to investigate PESs, followed by statistical calculations of reaction rate constants at temperatures relevant to combustion. All investigated pathways were shown to have reasonably low barriers (with respect to combustion conditions) for the reaction steps involved and, therefore, to represent potentially important contributors to the formation of indene.

In the present study, we focus on the indene formation mechanism originating from the reactions of two important cyclic C_5 species, **CPD** and **CPDyl**. The crucial role of these hydrocarbons in the formation of aromatics and PAHs growth in combustion has been suggested and then confirmed in numerous studies (see, for instance, ref 9 and references therein). The reaction mechanism starting from the intermolecular addition of **CPDyl** to a π bond of **CPD**, followed by rearrangements on the $C_{10}H_{11}$ PES and CH_3 elimination at the final step, producing indene, has been suggested by Wang et al. to explain the high indene yield in **CPD** pyrolysis.[5,6] They calculated a portion of the $C_{10}H_{11}$ PES shown in Scheme 1 at the B3LYP/6-31G(d,p) level and found reasonably low barriers (within 12−50 kcal/mol) for the reaction steps involved in the considered rearrangements, indicating that the suggested radical−molecule mechanism represents a significant contributor to the indene production in pyrolysis and combustion flames. However, the mechanism suggested by Wang et al. covers only a small part of the $C_{10}H_{11}$ isomerization network originating from the reactions between **CPD** and **CPDyl**. The complete network is

* To whom correspondence should be addressed. E-mail: mebela@fiu.edu.
[†] Permanent address: Institute of Solution Chemistry of Russian Academy of Sciences, 1 Akademicheskaya St., Ivanovo, 153045 Russia.

10.1021/jp077493f CCC: $40.75
Published on Web 01/09/2008

SCHEME 1: Rearrangements of the Initial Product (8,9,10-Trihydrofulvalenyl Radical) of the CPDyl + CPD Reaction Suggested and Computed by Wang et al.[6] at the B3LYP/6-31G Level**

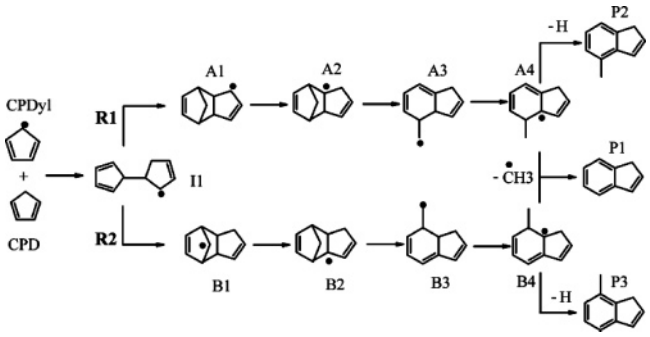

expected to be much more complicated, and other competitive pathways are possible, resulting in different reaction rates, reaction products, and relative product yields. Recently, we studied various rearrangements of the 9-H-fulvalenyl radical, which take place on the $C_{10}H_9$ PES.[10] This radical can also be produced by the reaction of **CPD** and **CPDyl** followed by the loss of two H atoms, and it can rearrange to azulene, naphthalene, and fulvalene. In the case of the $C_{10}H_{11}$ PES, the pathways leading to azulene-like products should also be taken into account because they may further contribute to the production of naphthalene by azulene−naphthalene isomerization.[10,11] Another issue concerns the role of **CPDyl** recombination in the formation of indene in combustion flames. Indeed, the recombination of two **CPDyl** produces 9,10-dihydrofulvalene **S0** (the numbering of carbon atoms used for various species discussed in this study is illustrated in Scheme 2) accessing the singlet $C_{10}H_{10}$ PES, and the recombination product then may easily react with an available H atom, producing the key intermediate I1 (8,9,10-trihydrofulvalenyl radical) shown in Scheme 1, which belongs to the $C_{10}H_{11}$ PES. Such a mechanism may give a significant contribution to the indene production in combustion flames, where the concentration of **CPDyl** is high, whereas the **CPD** + **CPDyl** reaction is more likely to occur in the pyrolytic conditions, where the concentration of **CPDyl** is expected to be substantially lower than that in combustion. With these considerations in mind, we performed an extensive investigation of various rearrangements on the $C_{10}H_{11}$ PES originating from both **CPD** + **CPDyl** and **CPDyl** + **CPDyl** reactions, applying the accurate G3(MP2,CC)//B3LYP technique followed by statistical calculations of reaction rate constants and relative product yields. The current study continues our previous theoretical investigations of various indene formation mechanisms[8] and also complements the recent study of 9-H-fulvalenyl radical rearrangements on the $C_{10}H_9$ PES,[10] which can also originate from the reactions involving **CPD** and **CPDyl**.

2. Computational Methods

In this study, we used the same computational technique as that in the previous part of this series;[8] therefore, we shall describe the computational technique briefly. The hybrid density functional B3LYP[12] method with the 6-311G** basis set was utilized for geometry optimization, calculation of harmonic frequencies, molecular structural parameters, and zero-point energy (ZPE) corrections. The G3(MP2,CC)//B3LYP modification[13] of the original Gaussian-3 (G3) scheme[14] was used to refine energies of all species. This G3-type calculation approach normally provides accuracies of 1−2 kcal/mol for relative energies of various stationary points on the PES, including transition states, unless a wave function has a strong multireference character. Multireference effects may be especially significant for species with open-shell singlet wave functions, which we do not encounter in this study. In general, the CCSD(T)-based methods, such as G3, are considered as an efficient, normally reliable, and uniform alternative to multireference calculations, applicable to moderately multireference wave functions,[15] especially where MRCI or CASPT2 calculations with appropriate active spaces are not feasible, as for the molecules considered here. The Gaussian 98[16] program package was used to carry out B3LYP and MP2 calculations, and the Molpro 2002[17] program package was employed to perform calculations of (R)/RCCSD(T) spin-restricted coupled cluster energies. Optimized Cartesian coordinates of all local minima and transition-state structures are collected in Table S1 of the Supporting Information, along with unscaled vibrational frequencies, moments of inertia, rotational constants, ZPE corrections, and B3LYP total energies at 0 K. The G3-computed relative energies, barrier heights, and heats of reactions (in kcal/mol) for all studied reactions are shown in Figures 1−5.

Thermal rate constants at the high-pressure limit were computed using the conventional RRKM[18−20] and TST[21] theories for unimolecular and bimolecular reactions, respectively. The partition functions were calculated using the harmonic oscillator approximation for vibrations and the rigid

SCHEME 2: The Notation of Carbon Atoms for Various Intermediates and Products Considered in the Present Study

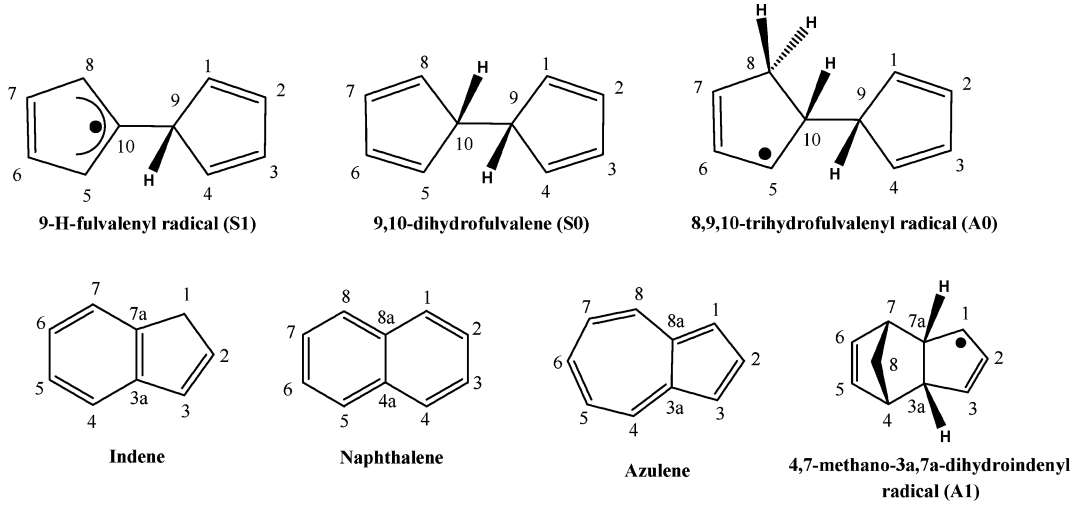

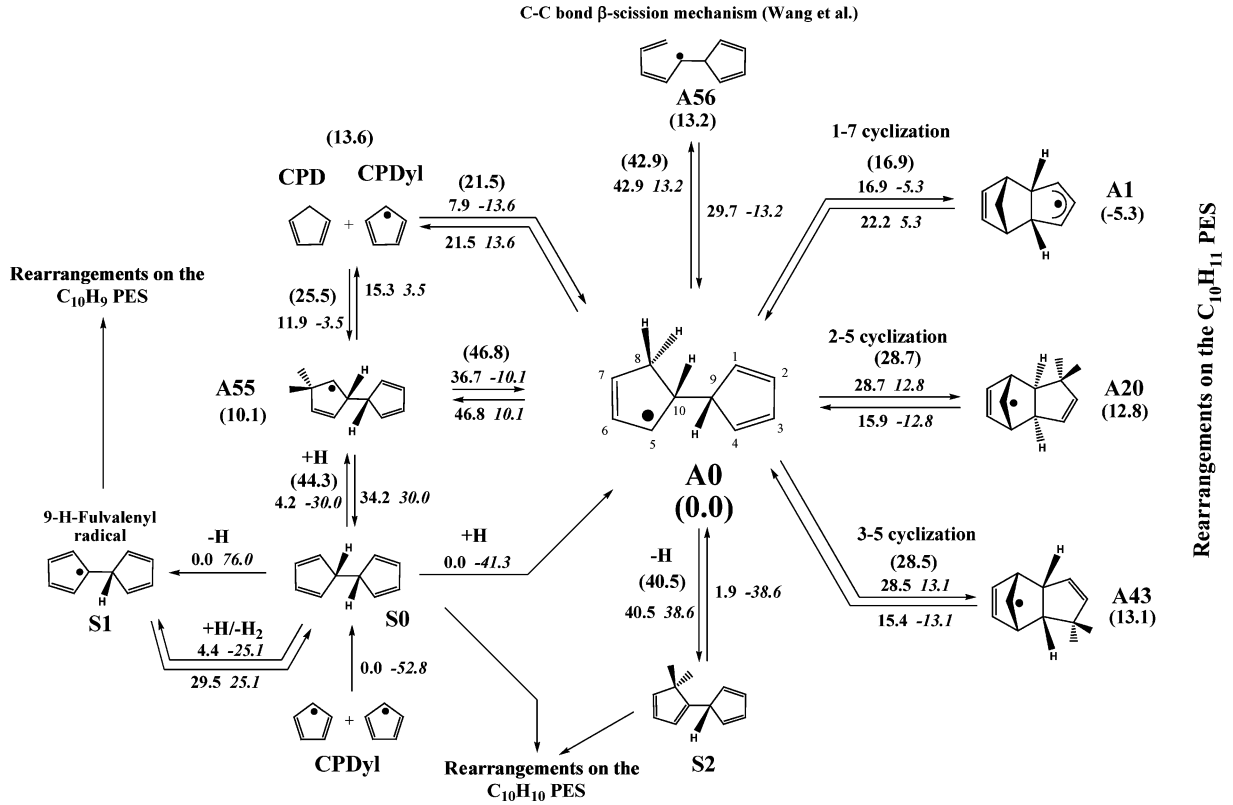

Figure 1. Possible rearrangements of reaction products of **CPDyl** recombination and the intermolecular addition of **CPDyl** to **CPD**. The numbers along the arrows show G3(MP2,CC)//B3LYP-computed barrier heights and heats of reactions (in italics) in kcal/mol. The numbers shown in parentheses represent the energies (kcal/mol) relative to **A0**.

rotor for rotational contributions. The direct count method based on the modified Beyer−Swinehart algorithm[18] was used in calculations of the number and densities of states in RRKM computations. Tunneling corrections to the rate constants were calculated using Wigner's formula.[18] All computed rate constants within the 300−3000 K temperature range are collected in Table S2 of the Supporting Information.

3. Results and Discussion

3.1. Reactions of CPDyl Self-Recombination and Intermolecular Addition of CPDyl to CPD. Possible mechanisms involving **CPD** and **CPDyl** under combustion and pyrolytic conditions are summarized in Figure 1. In general, reactions of **CPDyl** self-recombination and **CPDyl** addition to **CPD** can result in four possible products, 9,10-dihydrofulvalene (**S0**), the 9-H-fulvalenyl radical (**S1**), the 8,9,10-trihydrofulvalenyl radical (**A0**), and its structural isomer, the 7,9,10-trihydrofulvalenyl radical (**A55**). All of these species then may undergo various rearrangements on the $C_{10}H_{10}$ (**S0**), $C_{10}H_9$ (**S1**), and $C_{10}H_{11}$ (**A0** and **A55**) PESs, leading to the formation of various PAHs. The addition of **CPDyl** to **CPD** should be the more important reaction in pyrolysis of hydrocarbon fuels, such as **CPD**,[5,6] where the concentration of **CPDyl** is expected to be low, whereas in combustion flames, **CPDyl** self-recombination should be more significant. Rearrangements of 9,10-dihydrofulvalene **S0** on the singlet $C_{10}H_{10}$ PES have not been studied by theoretical methods so far; however, other important mechanisms taking place on this PES, involving azulene−naphthalene rearrangement, have been investigated by Alder et al. using a DFT method.[11] It is worth noting that $C_{10}H_{10}$ isomerizations exhibit high barriers, and therefore, the singlet surface mechanism is not likely to be competitive under combustion conditions, with the radical-promoted mechanisms occurring on the $C_{10}H_9$ and $C_{10}H_{11}$ PESs. Nevertheless, according to the alternative mechanism suggested by Carpenter, the isomerization of **S0** on the $C_{10}H_{10}$ PES may proceed via a tricyclic intermediate with a singlet biradical wave function, followed by ring opening to a 10-membered cyclic structure, which then rearranges to 4a,8a-dihydronaphthalene. The latter may produce naphthalene, eliminating a H_2 molecule. This pathway was not investigated so far by theoretical methods and is beyond the scope of the present study, but it will be reported in an upcoming publication.

The recombination product of two **CPDyl**'s, 9,10-dihydrofulvalene **S0**, is likely to react with a free H radical, a highly abundant radical in combustion flames; in pyrolysis, this mechanism is significantly less favorable because of a low H concentration. As follows from Figure 1, **S0** may undergo H atom-addition, producing the 8,9,10-trihydrofulvalenyl radical (**A0**) or its structural isomer, the 7,9,10-trihydrofulvalenyl radical (**A55**), or it may eliminate a hydrogen atom from the 9 or 10 positions directly or through a H-abstraction reaction, producing the 9-H-fulvalenyl radical **S1**. In the former case, one has to deal with rearrangements of **A0**/**A55** on the $C_{10}H_{11}$ PES (the subject of the present study), whereas in the latter case, the rearrangements on the $C_{10}H_9$ PES should be considered. Both addition and abstraction reactions involving **S0** are competitive from the energetic point of view. Although the addition **S0** → **A0** is barrierless (as confirmed by the PES scan), the competitive abstraction mechanism exhibits a low barrier of 4.4 kcal/mol and is strongly exothermic (to compare, the abstraction of a hydrogen atom from benzene requires a much higher barrier of 17 kcal/mol and is endothermic by 8.8 kcal/mol, as follows from our previous G3 study of the HACA mechanism[22]). The addition of a H atom to the alternative 7 position of **S0** also exhibits a low barrier of 4.2 kcal/mol, but it is less favorable than the

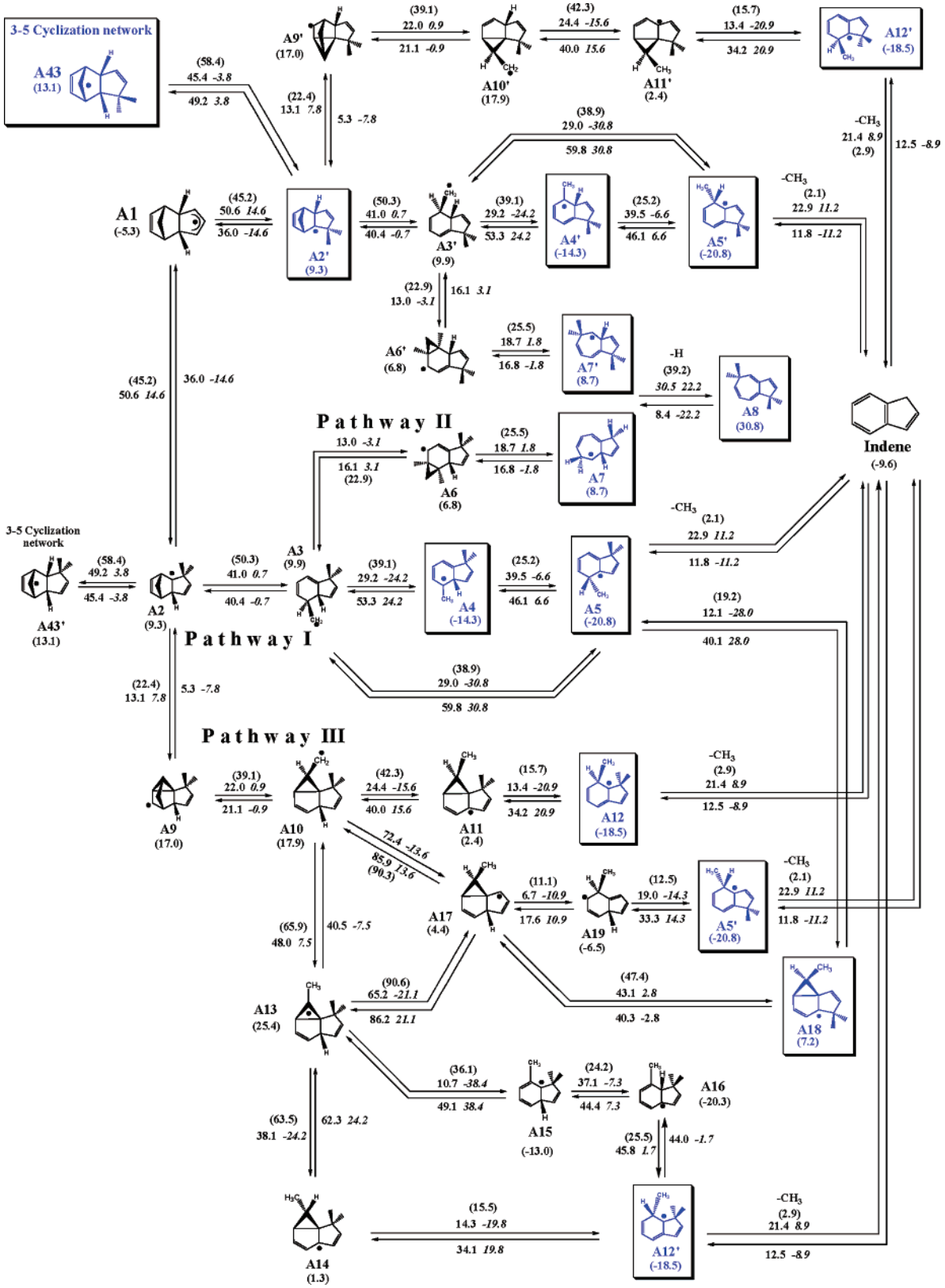

Figure 2. The 1−7 cyclization network for rearrangements of **A0**. The numbers along the arrows show G3(MP2,CC)//B3LYP-computed barrier heights and heats of reactions (in italics) in kcal/mol. The numbers shown in parentheses represent the energies (kcal/mol) relative to **A0**.

barrierless addition to the 8 position. The direct H elimination from **S0** requires 76 kcal/mol of energy, so that the $C_5H_5 + C_5H_5 \rightarrow$ **S0** $\rightarrow C_{10}H_9$ (**S1**) + H reaction is 23 kcal/mol endothermic and may play a certain role at high temperatures.

The rearrangements of the 9-H-fulvalenyl radical **S1** on the $C_{10}H_9$ PES were studied theoretically at different levels, initially by Melius and co-workers[23] applying the BAC-MP4 method and later by Wang et al.[6] and Alder et al.[11] using DFT methods. Recently, we revisited the **S1** isomerization mechanism utilizing the more accurate G3 technique combined with statistical calculations of rate constants and product branching ratios within the 300−3000 K temperature range at the high-pressure limit.[10]

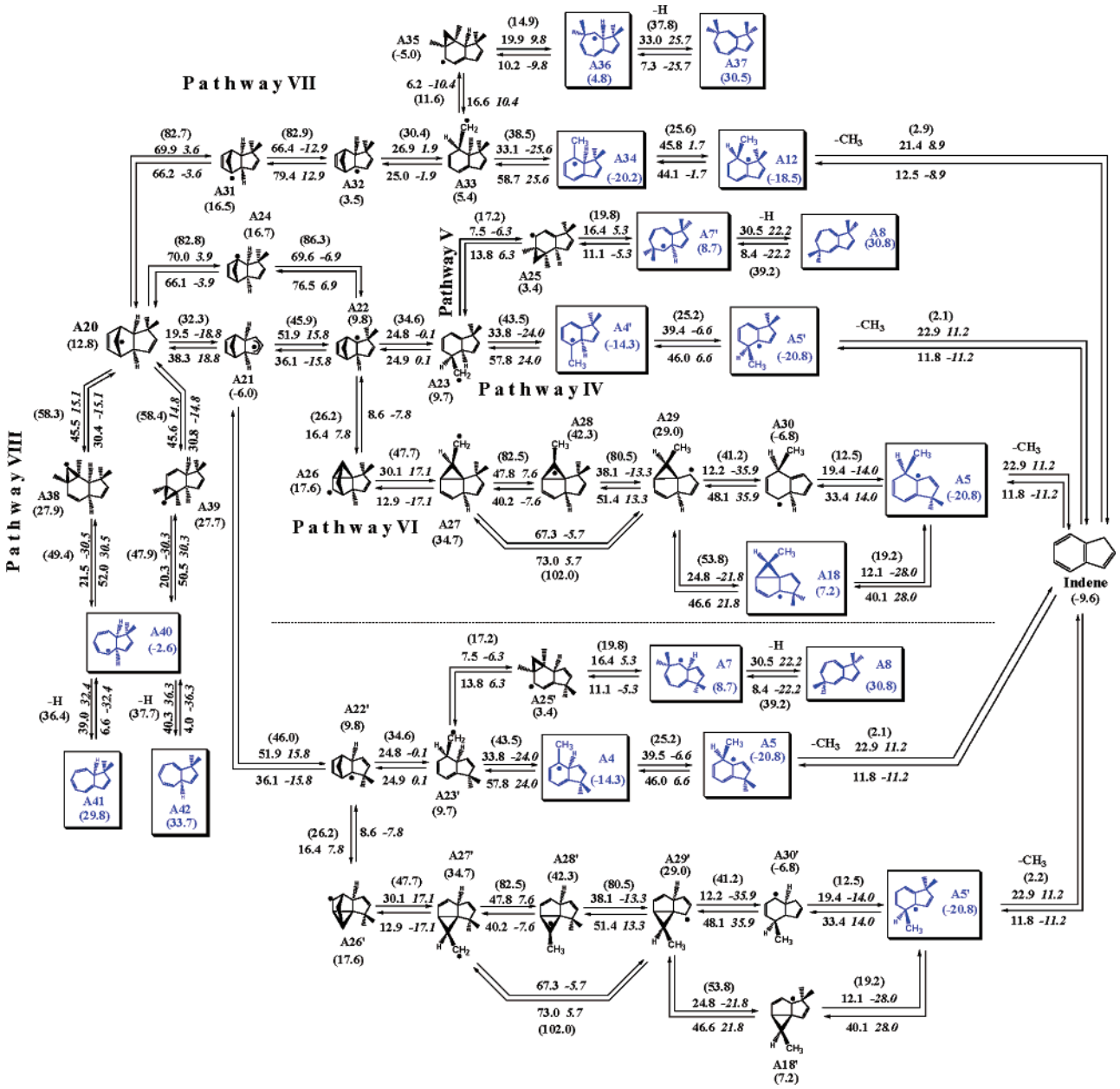

Figure 3. The 2−5 cyclization network for rearrangements of **A0**. The numbers along the arrows show G3(MP2,CC)//B3LYP-computed barrier heights and heats of reactions (in italics) in kcal/mol. The numbers shown in parentheses represent the energies (kcal/mol) relative to **A0**.

According to our results, naphthalene, fulvalene, and azulene are expected to be the reaction products, with the highest naphthalene yields (>50%) observed at low temperatures (T < 1000 K) corresponding to low-temperature pyrolytic conditions (e.g., **CPD** pyrolysis[5]). At higher temperatures corresponding to combustion conditions, the production of naphthalene rapidly decreases with increasing T, and fulvalene, a possible precursor of higher cyclopentafused PAHs, becomes the major reaction product. Starting from T = 1500 K, naphthalene and azulene together account for less than 10% of the total product yield. At all studied temperatures, the azulene yield does not exceed 5%, with the highest values (3.6−5%) calculated within the 1000−1500 K range.

The intermolecular addition of **CPDyl** to a π bond of **CPD** produces the 8,9,10-trihydrofulvalenyl radical **A0** or the 7,9,-10-trihydrofulvalenyl radical **A55**, and therefore, it directly accesses the $C_{10}H_{11}$ PES. The **A0** intermediate is 10.1 kcal/mol more stable than its isomer **A55**, and the barrier for the formation of the former (7.9 kcal/mol) is 4 kcal/mol lower than that for the latter (11.9 kcal/mol), indicating that the **CPD** + **CPDyl** → **A0** process is more energetically favorable. A comparison of individual bimolecular rate constants for the **CPD** + **CPDyl** → **A0** and **CPD** + **CPDyl** → **A55** steps shows that at temperatures relevant to combustion, the former reaction is 5−10 times faster than the latter (see Table 2). A similar relation is in effect for the rates of the reverse decomposition of **A0** and **A55**; the former dissociates to **CPD** + **CPDyl** 5−10 times slower than the latter. These results indicate that the major product of the radical−molecule reaction of **CPDyl** with **CPD** should be **A0**, which then undergoes rearrangements on the $C_{10}H_{11}$ PES. The contribution of the **CPD** + **CPDyl** → **A55** reaction is expected to be negligible at typical combustion temperatures. The **CPDyl** + **CPD** reaction was studied previously by Wang et al.[6] at the B3LYP/6-31G** level. Their B3LYP-calculated barrier and reaction exothermicity for the formation of **A0** (I1 in their original mechanism shown in Scheme 1) were 11.5 and 8.7 kcal/mol, respectively, which somewhat differ from our G3 results, 7.9 and 13.6 kcal/mol,

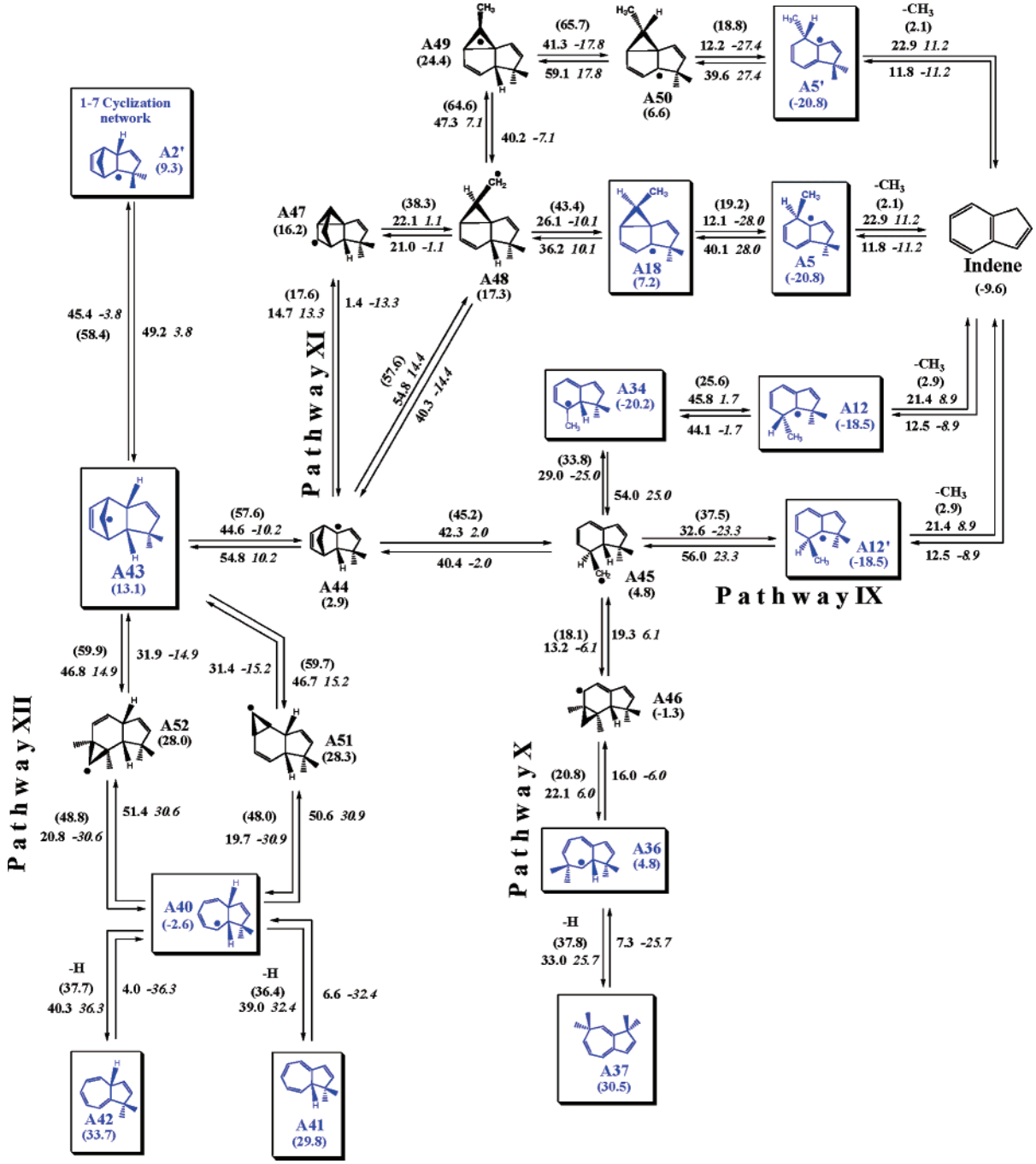

Figure 4. The 3−5 cyclization network for rearrangements of **A0**. The numbers along the arrows show G3(MP2,CC)//B3LYP-computed barrier heights and heats of reactions (in italics) in kcal/mol. The numbers shown in parentheses represent the energies (kcal/mol) relative to **A0**.

respectively (see Table 1). This discrepancy is within the margins expected between B3LYP and high-level model chemistry methods like G2 or G3. In addition to the rearrangements on the $C_{10}H_{11}$ PES shown in Scheme 1, Wang et al. investigated various pathways on the $C_{10}H_9$ PES leading from **A0** to naphthalene (via the **A0** → **S0** → **S1** sequence followed by the well-known spiran mechanism, initially suggested by Melius and co-workers[23]) and an alternative C−C bond β-scission pathway starting from the **A0** → **S56** reaction (shown in Figure 1), which involves a cleavage of the C_8-C_{10} bond in **A0** with further isomerization to naphthalene and benzene. Interestingly, for the H-atom addition to **S0**, **S0** + **H** → **A0**, they found a barrier of 0.5 kcal/mol, whereas according to our calculation at the higher B3LYP/6-311G** level, this reaction proceeds without a barrier, as confirmed by a careful PES scan.

The 8,9,10-trihydrofulvalenyl radical **A0** may further be involved in various rearrangements on the $C_{10}H_{11}$ PES, including several cyclizations, which are denoted as 1−7, 2−5, and 3−5 cyclizations in Figure 1. They produce the **A1**, **A20**, and **A43** tricyclic radical intermediates, respectively, with a 4−7 bridge. The competitive **A0** → **A55** isomerization exhibits a barrier of 36.7 kcal/mol, which is at least 8 kcal/mol higher than the cyclization barriers, especially for the 1−7 cyclization with a barrier of only 16.9 kcal/mol. The C−C bond β-scission pathway suggested previously by Wang et al.[6] starts from the **A0** → **A56** reaction, which also exhibits a significantly higher barrier of 42.9 kcal/mol (41.2 kcal/mol at the B3LYP level[6]), as well as the alternative elimination of a H atom from the 10 position of **A0**, producing 8,9-dihydrofulvalene **S2** with a barrier of 40.5 kcal/mol (45.1 kcal/mol at B3LYP[6]). The latter reaction is

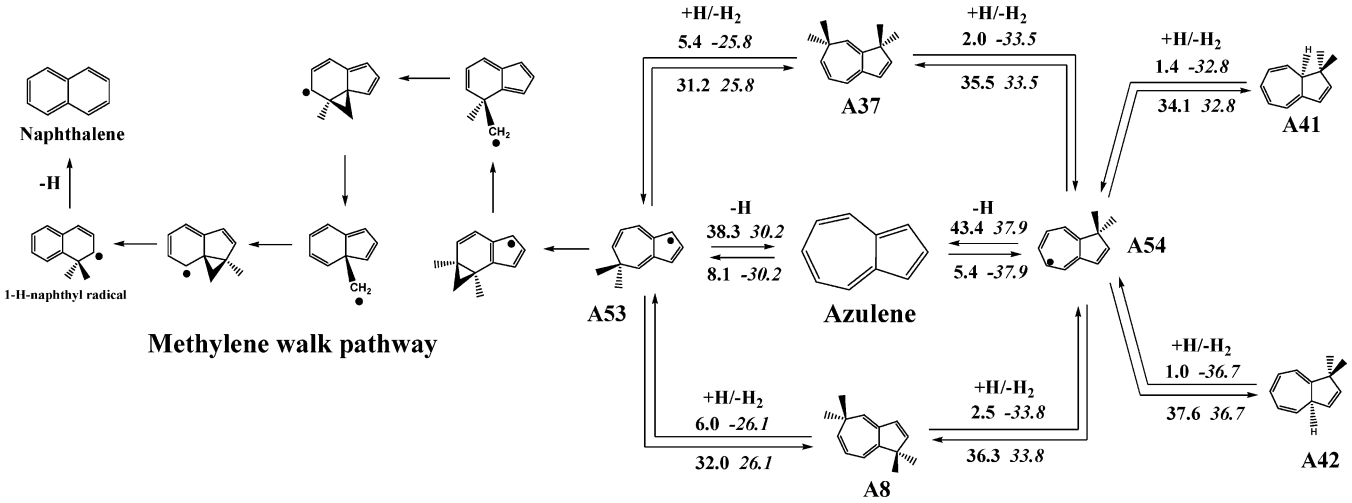

Figure 5. Possible mechanisms leading to azulene and naphthalene from 1,5-dihydroazulene **A8**, 1,7-dihydroazulene **A37**, 1,8a-dihydroazulene **A41**, and 1,3a-dihydroazulene **A42** formed by rearrangements of **A0**. The numbers along the arrows show G3(MP2,CC)//B3LYP-computed barrier heights and heats of reactions (in italics) in kcal/mol.

TABLE 1: Comparison of the G3-Computed Barrier Heights and Reaction Energies with the Values by Wang et al. Calculated at the B3LYP/6-31G Level[6]**

	barrier height, kcal/mol		heat of reaction, kcal/mol	
reaction	this study	Wang et al.	this study	Wang et al.
CPD + CPDyl → A0	7.9	11.5	−13.6	−8.7
A0 → A1	16.9	17.9	−5.3	0.0
A1 → A2	50.6	52.3	14.6	15.8
A2 → A3	41.0	37.9	0.7	−4.1
A3 → A5	29.0	25.3	−30.8	−37.8
A5 → indene	22.9	22.0	11.2	11.4
A0 → A43	28.5	32.1	13.1	22.3
A43 → A44	44.6	42.3	−10.2	−15.1
A44 → A45	42.3	38.2	2.0	−2.2
A45 → A12′	32.6	29.1	−23.3	−27.6
A12′ → indene	21.4	19.7	8.9	7.5

similar to the **A0 → S0** hydrogen elimination and leads to the singlet $C_{10}H_{10}$ PES. According to the calculated reaction energetics, the major **A0** consumption pathway should be **A0 → A1** (1−7 cyclization), with a barrier considerably lower than those for the other competing channels, including the alternative 2−5 and 3−5 cyclizations and, especially, the C−C bond β-scission route **A0 → A56**, isomerization to **A55**, and H-atom elimination **A0 → S2**. From this point of view, the role of the **CPDyl + CPD** reaction in the formation of the **S0** and **S1** species via the **A0 → S0** and **A55 → S0** H-elimination channels and, consequently, in rearrangements taking place on the $C_{10}H_{10}$ and $C_{10}H_9$ PESs should be insignificant. In the subsequent section, we describe all considered **A0** cyclization channels in more detail.

3.2. PES for Rearrangements of the 8,9,10-Trihydrofulvalenyl Radical A0. As shown on Figure 1, **A0** may undergo 1−7, 2−5, and 3−5 cyclizations, resulting in the formation of 4−7 bridged intermediates **A1**, **A20**, and **A43**, respectively. We also considered the possibility of alternative 1−6 and 4−6 cyclizations. However, the attempts to locate transition states for these reactions were unsuccessful; optimization always converged to the transition states corresponding to the 1−7, 2−5, or 3−5 cyclizations. The 1−7 cyclization produces the CH_2-bridged intermediate **A1**, with a barrier of only 16.9 kcal/mol and exothermicity of 5.3 kcal/mol, whereas the competitive 2−5 and 3−5 cyclizations lead to the formation of CH-bridged intermediates **A20** and **A43**, with notably higher barriers of 28.7 and 28.5 kcal/mol, respectively; in contrast to the **A0 → A1** reaction, the latter two cyclizations are endothermic by ∼13 kcal/mol. A comparison of individual rate constants for the **A0 → A1**, **A0 → A20**, and **A0 → A43** steps shown in Table 2 demonstrates that the first one is also more favorable kinetically at all studied temperatures. Indeed, the rate of the **A0 → A1** reaction is factors of 345, 48, and 18 faster than that of **A0 → A20** (2−5 cyclization) at 1000, 1500, and 2000 K, respectively, considering temperatures relevant to combustion. The rates of **A0 → A20** and **A0 → A43** are very close to each other at all studied temperatures because both reactions exhibit almost the same energetics. Although the **A0 → A1** reaction is much faster than its competitors, the relative contributions of the 2−5 and 3−5 cyclization channels are not insignificant since further isomerizations of **A1** exhibit higher barriers and lower rate constants, compared to the rearrangements of **A20** and **A43** (see section 3.4 for more detail).

The 1−7, 2−5, and 3−5 cyclization networks are depicted in Figures 2, 3, and 4, respectively. The reaction products include indene and several PAHs with one seven- and one five-membered ring fused together, 1,5-dihydroazulene **A8**, 1,7-dihydroazulene **A37**, 1,8a-dihydroazulene **A41**, and 1,3a-dihydroazulene **A42**. These azulene-like PAHs represent possible azulene precursors, which can produce this molecule after elimination of two H atoms (see discussion below). All three cyclization networks include numerous common intermediates (**A2′**, **A4**, **A4′**, **A5**, **A5′**, **A7**, **A7′**, **A12**, **A12′**, **A18**, **A34**, **A36**, **A40**, **A43**) and products (**A8**, **A37**, **A41**, **A42**), which are denoted with shadowed rectangular frames in the figures to make it easier to follow the considered mechanisms. A variety of optical isomers with the same energies can be also formed within the networks, and such isomers are marked with an apostrophe; for example, **A5** has an optical isomer **A5′**.

A. 1−7 Cyclization Network. The 1−7 cyclization network shown in Figure 2 starts either from 7a−1 or 3a−3 H migration with a relatively high barrier of 50.6 kcal/mol, resulting in formation of two optical isomers **A2** and **A2′**. The reaction is endothermic by 15.6 kcal/mol; therefore, the equilibrium at typical combustion temperatures (1000−2000 K) is shifted toward the **A1** adduct. This would reduce the contribution of the 1−7 cyclization network to the formation of indene and 1,5-dihydroazulene **A8**, despite the fact that the initial **A0 → A1** cyclization is significantly more energetically and kinetically favorable than the other competitive cyclizations. In contrast to the **A1 → A2** reaction, the respective **A20 → A21** and **A43**

TABLE 2: RRKM- and TST-Calculated High-Pressure-Limit Thermal Rate Constants (k, in Units of s^{-1} and $cm^3\ s^{-1}\ mol^{-1}$ for Unimolecular and Bimolecular Steps, Respectively) and Equilibrium Constants (K_{eq}) for Some Critical Reactions Involved in Rearrangements of the A0 Radical within the 500−3000 K Temperature Range

	temperature, K										
reactions	500	700	1000	1200	1400	1500	1700	2000	2400	2800	3000
k**(CPD + CPDyl → A0)**	4.3×10^5	6.8×10^6	7.2×10^7	2.0×10^8	4.6×10^8	6.6×10^8	1.2×10^9	2.5×10^9	5.6×10^9	1.1×10^{10}	1.4×10^{10}
k**(CPD + CPDyl → A55)**	4.8×10^3	2.3×10^5	5.7×10^6	2.2×10^7	6.4×10^7	1.0×10^8	2.1×10^8	5.4×10^8	1.4×10^9	3.0×10^9	4.1×10^9
k**(A0 → A1)**	1.5×10^4	1.7×10^6	6.1×10^7	2.4×10^8	6.6×10^8	9.9×10^8	1.9×10^9	4.0×10^9	8.1×10^9	1.3×10^{10}	1.6×10^{10}
k**(A0 → A20)**	1.2×10^{-1}	3.9×10^2	1.8×10^5	1.9×10^6	1.0×10^7	2.1×10^7	6.3×10^7	2.2×10^8	7.3×10^8	1.7×10^9	2.4×10^9
k**(A0 → A43)**	1.2×10^{-1}	3.9×10^2	1.7×10^5	1.8×10^6	9.5×10^6	1.9×10^7	5.7×10^7	2.0×10^8	6.5×10^8	1.5×10^9	2.1×10^9
K_{eq}**(A0 → A1)**	2.3	3.3×10^{-1}	7.6×10^{-2}	4.2×10^{-2}	2.8×10^{-2}	2.3×10^{-2}	1.8×10^{-2}	1.3×10^{-2}	9.6×10^{-3}	7.8×10^{-3}	7.1×10^{-3}
K_{eq}**(A0 → A20)**	9.5×10^{-8}	2.7×10^{-6}	3.3×10^{-5}	8.6×10^{-5}	1.7×10^{-4}	2.2×10^{-4}	3.5×10^{-4}	5.8×10^{-4}	9.3×10^{-4}	1.3×10^{-3}	1.5×10^{-3}
K_{eq}**(A0 → A43)**	5.2×10^{-8}	1.5×10^{-6}	1.9×10^{-5}	4.9×10^{-5}	9.7×10^{-5}	1.3×10^{-4}	2.0×10^{-4}	3.3×10^{-4}	5.3×10^{-4}	7.4×10^{-4}	8.5×10^{-4}
k**(A2 → A9)**	1.3×10^7	6.2×10^8	1.2×10^{10}	3.8×10^{10}	8.7×10^{10}	1.2×10^{11}	2.1×10^{11}	3.9×10^{11}	7.0×10^{11}	1.1×10^{12}	1.3×10^{12}
k**(A2 → A3)**	2.6×10^{-5}	5.1	5.1×10^4	1.9×10^6	2.5×10^7	7.1×10^7	3.9×10^8	2.7×10^9	1.6×10^{10}	6.1×10^{10}	1.0×10^{11}
k**(A2 → A43′)**	7.1×10^{-9}	9.1×10^{-3}	3.7×10^2	2.4×10^4	4.8×10^5	1.6×10^6	1.2×10^7	1.1×10^8	9.3×10^8	4.3×10^9	8.0×10^9
k**(A10 → A11)**	99	8.2×10^4	1.4×10^7	1.0×10^8	4.3×10^8	7.8×10^8	2.1×10^9	6.2×10^9	1.8×10^{10}	3.8×10^{10}	5.1×10^{10}
k**(A10 → A13)**	2.3×10^{-8}	2.0×10^{-2}	6.1×10^2	3.5×10^4	6.3×10^5	2.0×10^6	1.4×10^7	1.2×10^8	9.5×10^8	4.2×10^9	7.6×10^9
k**(A10 → A17)**	1.4×10^{-19}	1.1×10^{-10}	5.6×10^{-4}	2.4×10^{-1}	18	1.0×10^2	1.8×10^3	4.7×10^4	1.0×10^6	9.3×10^6	2.3×10^7
k**(A1 → A2)**[a]	3.4×10^{-9}	6.8×10^{-3}	3.8×10^2	2.8×10^4	6.0×10^5	2.1×10^6	1.6×10^7	1.6×10^8	1.4×10^9	6.7×10^9	1.3×10^{10}
k**(A20 → A21)**	1.7×10^4	3.6×10^6	2.2×10^8	1.1×10^9	3.6×10^9	5.9×10^9	1.3×10^{10}	3.2×10^{10}	7.5×10^{10}	1.4×10^{11}	1.8×10^{11}
k**(A21 → A22)**	5.0×10^{-10}	1.5×10^{-3}	1.1×10^2	8.9×10^3	2.1×10^5	7.4×10^5	6.0×10^6	6.3×10^7	5.9×10^8	3.0×10^9	5.7×10^9
K_{eq}**(A1 → A2)**	4.8×10^{-7}	3.1×10^{-5}	7.1×10^{-4}	2.4×10^{-3}	5.6×10^{-3}	7.9×10^{-3}	1.4×10^{-2}	2.6×10^{-2}	4.9×10^{-2}	7.5×10^{-2}	8.9×10^{-2}
K_{eq}**(A20 → A21)**	9.5×10^7	3.9×10^5	6.2×10^3	1.2×10^3	3.9×10^2	2.5×10^2	1.2×10^2	50	22	12	9.9
k**(A23 → A25)**	$1{,}4 \times 10^9$	$1{,}2 \times 10^{10}$	$5{,}7 \times 10^{10}$	$1{,}1 \times 10^{11}$	$1{,}7 \times 10^{11}$	$2{,}0 \times 10^{11}$	$2{,}7 \times 10^{11}$	$3{,}8 \times 10^{11}$	$5{,}3 \times 10^{11}$	$6{,}6 \times 10^{11}$	$7{,}2 \times 10^{11}$
k**(A23 → A4′)**	$3{,}9 \times 10^{-2}$	$5{,}9 \times 10^2$	$8{,}7 \times 10^5$	$1{,}5 \times 10^7$	$1{,}2 \times 10^8$	$2{,}7 \times 10^8$	$1{,}1 \times 10^9$	$5{,}1 \times 10^9$	$2{,}2 \times 10^{10}$	$6{,}4 \times 10^{10}$	$9{,}7 \times 10^{10}$
k**(A25 → A7′)**	$8{,}3 \times 10^5$	$1{,}2 \times 10^8$	$4{,}8 \times 10^9$	$2{,}1 \times 10^{10}$	$5{,}7 \times 10^{10}$	$8{,}9 \times 10^{10}$	$1{,}8 \times 10^{11}$	$3{,}9 \times 10^{11}$	$8{,}2 \times 10^{11}$	$1{,}4 \times 10^{12}$	$1{,}7 \times 10^{12}$
k**(A4′ → A5′)**	$1{,}6 \times 10^{-4}$	13	$6{,}3 \times 10^4$	$1{,}8 \times 10^6$	$2{,}0 \times 10^7$	$5{,}3 \times 10^7$	$2{,}6 \times 10^8$	$1{,}6 \times 10^9$	$8{,}8 \times 10^9$	$3{,}0 \times 10^{10}$	$4{,}9 \times 10^{10}$
k**(A22 → A26)**	$3{,}8 \times 10^5$	$4{,}9 \times 10^7$	$1{,}9 \times 10^9$	$8{,}0 \times 10^9$	$2{,}2 \times 10^{10}$	$3{,}4 \times 10^{10}$	$6{,}7 \times 10^{10}$	$1{,}4 \times 10^{11}$	$3{,}0 \times 10^{11}$	$5{,}0 \times 10^{11}$	$6{,}1 \times 10^{11}$
k**(A22 → A23)**	$2{,}2 \times 10^2$	$3{,}9 \times 10^5$	$1{,}1 \times 10^8$	$1{,}0 \times 10^9$	$5{,}2 \times 10^9$	$9{,}8 \times 10^9$	$2{,}8 \times 10^{10}$	$9{,}2 \times 10^{10}$	$2{,}9 \times 10^{11}$	$6{,}4 \times 10^{11}$	$8{,}8 \times 10^{11}$
k**(A43 → A44)**	$6{,}4 \times 10^{-7}$	$2{,}1 \times 10^{-1}$	$2{,}9 \times 10^3$	$1{,}3 \times 10^5$	$1{,}9 \times 10^6$	$5{,}5 \times 10^6$	$3{,}3 \times 10^7$	$2{,}5 \times 10^8$	$1{,}7 \times 10^9$	$6{,}8 \times 10^9$	$1{,}2 \times 10^{10}$
k**(A44 → A45)**	$5{,}1 \times 10^{-6}$	1,4	$1{,}8 \times 10^4$	$7{,}4 \times 10^5$	$1{,}0 \times 10^7$	$3{,}0 \times 10^7$	$1{,}7 \times 10^8$	$1{,}3 \times 10^9$	$8{,}1 \times 10^9$	$3{,}1 \times 10^{10}$	$5{,}2 \times 10^{10}$
k**(A20 → A31)**	$5{,}7 \times 10^{-18}$	$2{,}6 \times 10^{-9}$	$8{,}6 \times 10^{-3}$	3,0	$2{,}0 \times 10^2$	$1{,}1 \times 10^3$	$1{,}8 \times 10^4$	$4{,}2 \times 10^5$	$8{,}2 \times 10^6$	$7{,}0 \times 10^7$	$1{,}6 \times 10^8$
k**(A31 → A32)**	$2{,}9 \times 10^{-16}$	$5{,}63 \times 10^{-8}$	$9{,}9 \times 10^{-2}$	28	$1{,}6 \times 10^3$	$8{,}1 \times 10^3$	$1{,}2 \times 10^5$	$2{,}4 \times 10^6$	$4{,}3 \times 10^7$	$3{,}4 \times 10^8$	$7{,}8 \times 10^8$
k**(A20 → A38)**	$1{,}6 \times 10^{-7}$	$9{,}1 \times 10^{-2}$	$2{,}0 \times 10^3$	$9{,}7 \times 10^4$	$1{,}6 \times 10^6$	$4{,}8 \times 10^6$	$3{,}0 \times 10^7$	$2{,}4 \times 10^8$	$1{,}7 \times 10^9$	$7{,}0 \times 10^9$	$1{,}2 \times 10^{10}$
k**(A20 → A39)**	$1{,}4 \times 10^{-7}$	$8{,}2 \times 10^{-2}$	$1{,}8 \times 10^3$	$9{,}0 \times 10^4$	$1{,}5 \times 10^6$	$4{,}5 \times 10^6$	$2{,}8 \times 10^7$	$2{,}3 \times 10^8$	$1{,}6 \times 10^9$	$6{,}5 \times 10^9$	$1{,}2 \times 10^{10}$

[a] Rate constants are multiplied by a factor of 2 to take into account both **A1 → A2** and **A1 → A2′** reactions.

→ A44 reactions, which start competitive isomerizations of the **A20** and **A43** adducts within the 2−5 and 3−5 cyclization networks, respectively, exhibit lower barriers and are exothermic. Since **A2** and **A2′** are optical isomers, the further rearrangements involve two energetically equivalent reaction sequences with similar reaction steps, the same energetics, and optical isomers as intermediates. Hence, we discuss only one of them starting from **A2**.

The further rearrangements of the **A2** radical involve three major pathways. The first one, **A2 → A3 → A5 → indene** (pathway I), begins with a cleavage of the C_7-C_8 bond of the 4−7 CH_2 bridge, **A2 → A3**, leading to the bicyclic structure **A3** with an indene core via a 41 kcal/mol barrier and an exothermicity of only 0.7 kcal/mol. Note that the scission of an alternative C_4-C_8 bond in **A2** produces a triradical structure, which is energetically unfavorable and therefore is not considered here. Then, after migration of the H atom linked to the 3a carbon to the methylene group connected to the 4 carbon, **A3 → A5**, with a barrier of 29 kcal/mol and high exothermicity of 30.8 kcal/mol, the **A5** radical (20.8 kcal/mol more stable than the initial **A0** adduct) undergoes methyl group elimination, yielding indene. The last step has a relatively low barrier of 22.9 kcal/mol and is endothermic by 11.2 kcal/mol. We also considered an alternative **A3 → A4 → A5** sequence, which involves two consecutive H migrations **A3 → A4** and **A4 → A5**, with barriers of 29.2 and 39.5 kcal/mol, respectively. Although the first step exhibits almost the same barrier as that of the **A3 → A5** H migration (but 6.6 kcal/mol lower exothermicity), the second 3a−4 H shift **A4 → A5** has a high barrier of 39.5 kcal/mol, which makes the **A3 → A4 → A5** sequence hardly competitive with the one-step **A3 → A5** mechanism. The **A0 → A1 → A2 → A3 → A5 → indene** mechanism was previously calculated at the B3LYP/6-31G(d,p) level by Wang et al.[6] (shown in Scheme 1 as route R1), and here, we refined geometries of all species at the higher B3LYP/6-311G** level and calculated reaction barriers and energies using the more accurate G3 method. As follows from their original reaction scheme shown in Scheme 1, the **I1 → A1** reaction corresponds to 1−7 cyclization **A0 → A1**, and the **A1 → A2 → A3 → A4 → P1** sequence shown in Scheme 1 is the same as our computed **A1 → A2 → A3 → A5 → indene** pathway shown in Figure 2. A comparison of our G3-calculated barriers and reaction energies for this pathway with the B3LYP results of Wang and co-workers presented in Table 1 shows a general agreement within ∼1−4 kcal/mol for barriers and ∼7 kcal/mol for reaction energies.

In the second pathway **A3 → A6 → A7 → A8** (pathway II), the **A3** adduct undergoes a cyclization process involving the methylene group linked to the 4 carbon and produces tricyclic intermediate **A6** with a barrier of only 13 kcal/mol and an exothermicity of 3.1 kcal/mol. The subsequent expansion of the six-membered ring in **A6** leads to the formation of the 1,3a,5-trihydroazulyl radical **A7** (azulene core) with a barrier of 18.7 kcal/mol, which then undergoes H-atom elimination, producing 1,5-dihydroazulene **A8**, a possible azulene precursor. The last step exhibits a 30.5 kcal/mol barrier and is 22.2 kcal/mol endothermic, which is typical for H-atom elimination from PAH radicals.[8,10,22] This pathway is more energetically favorable than pathway I because the starting **A3 → A6** cyclization step has a barrier 16 kcal/mol lower as compared to that for the competing **A3 → A5** H migration.

Similar to pathway I, the third pathway **A2 → A9 → A10 → A11 → A12 → indene** (pathway III) leads to indene and is actually the most energetically favorable mechanism within the

1−7 cyclization network. In the initial **A2** → **A9** step, the six-membered ring of **A2** transforms to one five- and one three-membered ring, producing intermediate **A9** with a $CH-CH_2$ bridge. This step exhibits a low barrier of 13.1 kcal/mol and therefore is more favorable than the competing **A2** → **A3** reaction. The further rearrangements also proceed with relatively low barriers and include the C−C bond scission **A9** → **A10** (a barrier of 22 kcal/mol), producing the tricyclic structure **A10**, followed by H migration **A10** → **A11** with a barrier of 24.4 kcal/mol and an expansion of the five-membered ring in **A11,** producing an indene core in the **A12** radical with a barrier of 13.4 kcal/mol and a high exothermicity of 20.9 kcal/mol. The H migration to the methylene group **A10** → **A11** is required prior to expansion of the five-membered ring; otherwise, the ring expansion would lead to an energetically unfavorable triradical structure. Similar to the **A5** radical, **A12** is a very stable intermediate within the network (18.5 kcal/mol lower in energy than the initial **A0** radical). Indene can be formed after elimination of the methyl group from **A12**, with a barrier of 21.4 kcal/mol and endothermicity of 8.9 kcal/mol, which are close to the respective values for the CH_3 group loss from the **A5** radical, 22.9 and 11.2 kcal/mol. We also investigated alternative rearrangements of the tricyclic structure **A10** leading to indene, starting from H-atom migrations **A10** → **A13** and **A10** → **A17**. These reactions make possible an expansion of the five-membered ring after a H atom migrates to methylene, forming a methyl group. Indeed, the subsequent **A17** → **A19**, **A13** → **A15**, and **A14** → **A12′** ring expansions producing an indene core exhibit low barriers of 6.7, 10.7, and 14.3 kcal/mol, respectively. However, the computed barriers for both **A10** → **A13** and **A10** → **A17** H-migration steps are significantly higher (48 and 72.4 kcal/mol, respectively) than the 24.4 kcal/mol barrier for the competing **A10** → **A11** H migration. This makes the former two reactions energetically unfavorable as compared to the latter. Calculations of rate constants and relative product yields discussed in section 3.4 also confirm that the contributions of the alternative channels starting from the **A10** → **A13** and **A10** → **A17** steps to the total product yield are negligible.

In addition to the previously discussed pathways I−III, the **A2** and **A2′** adducts may also rearrange to **A43′** and **A43** by migration of a hydrogen atom from the bridge CH_2 group to 3a or 7a positions of **A2′** or **A2**, respectively. Because the **A43** adduct can be also formed by a 3−5 cyclization of the initial **A0** radical, **A0** → **A43** (see Figure 1), the **A2** → **A43′** and **A2′** → **A43** reactions directly connect two cyclization networks. On the other hand, the **A2** → **A43′** and **A2′** → **A43** reactions exhibit a barrier that is 36 kcal/mol higher than that for the competing **A2** → **A9** step, which starts pathway III. As a result, calculated rate constants for the **A2** → **A43′** and **A2′** → **A43** steps at typical combustion temperatures are several orders of magnitude lower than those for **A2** → **A9** (see Table 2), and hence, the consumption of **A2**/**A2′** radicals by the **A2** → **A43′** and **A2′** → **A43** reactions is expected to be negligible (the reverse reactions, however, are more likely to take place).

A comparison of respective barriers and rate constants for the competing **A2** → **A9** and **A2** → **A3** reactions shows that the former is more kinetically favorable. Indeed, the **A2** → **A3** step has a 28 kcal/mol higher barrier as compared to that of the **A2** → **A9** reaction, and the rate constants for the former are about 6, 3, and 2 orders of magnitude lower than those for the latter at 1000, 1500, and 2000 K, respectively. This indicates that pathway III is the dominant isomerization mechanism within the 1−7 cyclization network, whereas the contributions of pathway I previously suggested by Wang et al.[6] and the alternative pathway II leading to 1,5-dihydroazulene **A8** are expected to be low.

B. 2−5 Cyclization Network. The 2−5 cyclization network shown in Figure 3 involves a number of pathways, which are similar to the previously discussed mechanisms for the 1−7 cyclization network. Unlike 1−7 cyclization, 2−5 cyclization **A0** → **A20** leads to the formation of the 4−7 CH-bridged radical **A20** with an unpaired electron localized on the CH bridge. The **A20** adduct may further isomerize to CH_2-bridged structures **A21**, **A24**, and **A31** via 1−8, 7−8, and 4−8 H migrations, respectively, or rearrange to tricyclic structures **A38** and **A39**, with subsequent ring expansion producing an azulene core in **A40**. According to the calculated energetics, the 1−8 H migration **A20** → **A21** with a 19.5 kcal/mol barrier is significantly more favorable than the alternative 7−8 **A20** → **A24** and 4−8 **A20** → **A31** H migrations exhibiting very high barriers of ∼70 kcal/mol, as well as the **A20** → **A38** and **A20** → **A39** rearrangements with barriers of ∼45.5 kcal/mol. Also, the **A20** → **A21** reaction is 18.8 kcal/mol exothermic, whereas all competing steps are endothermic. The **A21** structure is very similar to that of **A1**, which starts the 1−7 cyclization network shown in Figure 2, except that the H atoms sitting at the 3a and 7a positions in **A21** are pointed in the opposite direction as compared to those in **A1**. As a result, both intermediates **A1** and **A21** have close relative energies of −5.3 and −6 kcal/mol, respectively, and further rearrangements of **A21** are also similar to the previously discussed pathways I−III in the 1−7 cyclization network, with some important exceptions. Indeed, pathways IV, V, and VI shown in Figure 3 involve reaction steps and structures, which are similar to those observed in pathways I, II, and III, respectively. Like in the 1−7 cyclization network, there are two energetically equivalent subnetworks with optical isomers initiated by the **A21** → **A22** and **A21** → **A22′** steps.

The calculated energetics of pathway IV, **A22** → **A23** → **A4′** → **A5′** → **indene**, is very similar to that for the **A2** → **A3** → **A4** → **A5** → **indene** sequence within pathway I in the 1−7 cyclization network. The only exception is the C_4-C_8 bond-breaking step **A22** → **A23**, which has a barrier almost a factor of 2 lower than that for **A2** → **A3**. A comparison of relative energies for all species involved in these two steps shows that the large difference in the calculated barriers originates from the energy difference for the two respective transition states; the transition state for **A2** → **A3** is 15.7 kcal/mol higher in energy (50.3 kcal/mol) than that for **A22** → **A23** (34.6 kcal/mol), whereas the relative energies of the **A2** and **A22** reactants are very close to each other, 9.3 and 9.8 kcal/mol, respectively. The relative energies of the reaction products **A3** and **A23** are also similar, 9.9 and 9.7 kcal/mol, respectively. Interestingly, both transition states exhibit similar imaginary frequencies of 629i and 605i, as well as the distances for the breaking C−C bonds of 2.3 and 2.2 Å for **A2** → **A3** and **A22** → **A23**, respectively. The formation of the **A22** intermediate from the initial **A20** adduct can be accomplished via two routes, **A20** → **A21** → **A22** and **A20** → **A24** → **A22**. The former involves 1−8 H migration **A20** → **A21** with a small barrier of 19.5 kcal/mol, whereas the latter proceeds via 7−8 H migration **A20** → **A24**, which requires overcoming a high barrier of 70 kcal/mol, followed by the subsequent **A24** → **A22** 7a−7 H shift with a barrier as high, 69.6 kcal/mol. This means that the **A20** → **A24** → **A22** sequence is unlikely to compete with **A20** → **A21** → **A22** and can be neglected. The crucial difference between pathways I and IV is that in the case of the latter, the direct

A23 → **A5′** H migration is impossible because the H atom in **A23** linked to the 3a carbon and the methylene group linked to the 4 carbon have opposite orientations (structures are shown in Table S1 of the Supporting Information). Owing to this structural feature of **A23**, pathway IV involves an extra 3a−4 hydrogen shift **A4′** → **A5′** with a high barrier of 39.4 kcal/mol, similar to the energetically unfavorable **A3** → **A4** → **A5** sequence considered for pathway I. This renders pathway IV less energetically favorable as compared to the similar pathway I in the 1−7 cyclization network.

The **A23** → **A25** → **A7′** → **A8** sequence denoted as pathway V in Figure 3 is similar to pathway II (Figure 2) and also leads to the formation of an azulene precursor **A8** (1,5-dihydroazulene). In contrast to pathway II, the initial **A23** → **A25** step producing a tricyclic structure **A25** exhibits an almost twice lower barrier of 7.5 kcal/mol and a higher exothermicity as compared to the respective **A3** → **A6** step with a barrier of 13 kcal/mol. The subsequent **A25** → **A7′** ring expansion also shows a slightly lower (by 2.3 kcal/mol) barrier as compared to that of the related **A6** → **A7** expansion within pathway II. The barrier of the **A23** → **A25** reaction is also a factor of 4.5 lower than the barrier for the competing **A23** → **A4′** H migration, indicating that pathway V is more favorable than pathway IV producing indene. As will be shown in section 3.4, pathway V provides a major contribution to the production of the azulene precursor **A8**. The large differences in the reaction barriers for **A22** → **A23** and **A23** → **A25** as compared to those for the analogous **A2** → **A3** and **A3** → **A6** steps, respectively, indicate that pathways IV and V within the 2−5 cyclization network represent more favorable alternatives to similar pathways I and II considered for 1−7 cyclization (note that this conclusion is relevant only for rearrangements within each network but not for the whole mechanism). Interestingly, pathways IV and V were not considered in the previous DFT study of Wang and co-workers,[6] who only suggested pathway I leading to indene (route R1 in Scheme 1). However, according to the present results, this route is substantially less energetically favorable within the 1−7 cyclization network as compared to the alternative pathway III.

Pathway VI starts from the formation of intermediate **A26** with a CH−CH_2 bridge, and obviously, this pathway is similar to pathway III considered for 1−7 cyclization from a structural point of view. However, from the energetic point of view, pathway VI is significantly less favorable than its analogue. Although the initial **A22** → **A26** reaction exhibits a barrier of 16.4 kcal/mol, which is close to the 13.1 kcal/mol barrier for the similar **A2** → **A9** step, the further rearrangements of the **A26** radical involve reaction steps with significantly higher barriers as compared to those for pathway III. The **A26** → **A27** bond scission process exhibits a 30.1 kcal/mol barrier, which is 12.1 kcal/mol higher than the respective barrier of 22 kcal/mol for the similar **A9** → **A10** reaction. The further isomerization of **A27** to indene proceeds via expansion of the five-membered ring, which requires a prior H migration to the radical site of **A27** localized on the CH_2 group. In contrast to pathway III, in the case of pathway VI, this may be accomplished only by energetically unfavorable 7−8 or 1−8 H migrations (**A27** → **A28** and **A27** → **A29**, respectively) with high barriers of 47.8 and 67.3 kcal/mol, respectively. The 3a−8 H migration is impossible in **A27** because of structural considerations; the CH_2 group and the H atom to be moved point in opposite directions. In **A10**, 3a−8 H shift **A10** → **A11** is feasible and exhibits a reasonably low barrier of 24.4 kcal/mol. Subsequent rearrangements of **A29** leading to the formation of an indene core in **A5** via five-membered ring expansion exhibit low barriers but involve two steps, **A29** → **A30** → **A5** or **A29** → **A18** → **A5**; in pathway III, the **A11** → **A12** ring expansion leads directly to the formation of an indene precursor **A12**. A comparison of pathways IV, V, and VI shows that although the initial **A22** → **A26** reaction in pathway VI exhibits a barrier that is 8.4 kcal/mol lower than that for the competing **A22** → **A23** bond scission, which starts both pathways IV and V, the further rearrangements within pathway VI involve more reaction steps with significantly higher barriers as compared to those for alternative pathways IV and V. All of these facts indicate that in contrast to pathway III, which is the most energetically favorable mechanism within the 1−7 cyclization network, pathway VI is not competitive with more favorable pathways IV and V in the 2−5 cyclization network. This conclusion will be illustrated on the basis of calculated product yields in section 3.4.

Pathway VII includes two reaction sequences, **A32** → **A33** → **A34** → **A12** → **indene** and **A32** → **A33** → **A35** → **A36** → **A37**, which are respectively similar to pathways IV and V discussed above. The latter mechanism leads to another azulene precursor **A37** (1,7-dihydroazulene), whereas the former sequence produces indene. Although both sequences exhibit reasonably low barriers similar to those in pathways IV and V, the two preceding H shifts **A20** → **A31** and **A31** → **A32**, which initiate pathway VII, display very high barriers of 69.9 and 66.4 kcal/mol, respectively. Such high barriers result in low rate constants for these two consecutive steps and make this mechanism very unfavorable both energetically and kinetically as compared to alternative pathways IV and V.

The last mechanism considered for the 2−5 cyclization network denoted as pathway VIII in Figure 3 involves two similar isomerizations **A20** → **A38** or **A20** → **A39** with almost the same barriers of ∼45.5 kcal/mol. The tricyclic structures **A38** and **A39** then undergo ring expansion, both producing an azulene core in **A40** (1,3a,8a-trihydroazulyl radical). The **A38** → **A40** and **A39** → **A40** ring expansions exhibit 21.5 and 20.3 kcal/mol barriers and are strongly exothermic, by 30.5 and 30.3 kcal/mol, respectively. The subsequent elimination of a hydrogen atom sitting either at the 3a or 8a positions requires overcoming a barrier of ∼40 kcal/mol, producing 1,8a-dihydroazulene **A41** or 1,3a-dihydroazulene **A42**, respectively. Since the initial **A20** → **A38** or **A20** → **A39** steps are ∼15 kcal/mol endothermic and their barriers are 26 kcal/mol higher than that for the competing 1−8 H migration **A20** → **A21**, which is, in contrast, 18.8 kcal/mol exothermic, we expect pathway VIII to be significantly less favorable than pathways IV and V within the 2−5 cyclization network.

C. 3−5 Cyclization Network. Reaction mechanisms in the 3−5 cyclization network shown in Figure 4 are akin to those considered for 1−7 and 2−5 cyclizations, but, again, some important exceptions take place. Since the **A0** → **A20** and **A0** → **A43** cyclizations lead to similar structures **A20** and **A43**, one can expect that subsequent rearrangements of both **A20** and **A43** should have similar mechanisms and energetics. Indeed, pathways IX, X, XI, and XII found in the 3−5 cyclization network are similar to previously discussed pathways I/IV, II/V, III/VI, and VII, respectively, considered for the 1−7 and 2−5 cyclization networks. The crucial distinction between the 3−5 and 2−5 cyclization routes is that in **A43**, the 3−8 H migration is prohibited because of unfavorable stereochemistry, whereas in **A20**, the analogous 1−8 H migration **A20** → **A21** is feasible and exhibits a low barrier of 19.5 kcal/mol. The **A43** adduct can undergo only 3a−8 **A43** → **A2′** or 7a−8 **A43** →

A44 H migrations, producing CH_2-bridged structures via relatively high barriers of 45.4 and 44.6 kcal/mol, respectively, which are more than a factor of 2 higher than the respective barrier for the **A20** → **A21** reaction. The alternative rearrangements of the **A43** adduct, **A43** → **A51** and **A43** → **A52**, lead to the tricyclic structures **A51** and **A52** (akin to pathway VIII) and also exhibit high barriers of ~47 kcal/mol. This means that possible isomerizations of **A43** within the 3−5 cyclization network involve energetically unfavorable steps with barriers of 45−47 kcal/mol, whereas **A20** rearranges to the CH_2-bridged intermediate **A21** by the favorable 1−8 H shift. From this point of view, the 2−5 cyclization route is preferable as compared to 3−5 cyclization, and this is confirmed by significantly lower relative contributions of the pathways shown in Figure 4 to the total product yields (see discussion in section 3.4). To understand why the 3−8 H migration is impossible in the **A43** radical, one has to compare the molecular structures of the **A20** and **A43** radicals shown in Table S1 of the Supporting Information. **A20** has a chair-like structure with the CH bridge located close to the CH_2 fragment of the cyclopenta ring; this makes the 1−8 H shift sterically possible. In contrast, **A43** possesses a boat-like structure where the CH bridge and CH_2 fragment of the cyclopenta ring are separated by a long distance and, more important, are sterically hindered; this makes the 3−8 hydrogen migration unfeasible.

Pathway IX, **A43** → **A44** → **A45** → **A12′** → **indene**, is akin to the **A2** → **A3** → **A5** → **indene** sequence (pathway I within the 1−7 cyclization network) shown in Figure 2. The barriers and reaction energies for **A44** → **A45**, **A45** → **A12′**, and **A12′** → **indene** reactions are very close (within 1−3 kcal/mol) to the corresponding values for the similar **A2** → **A3**, **A3** → **A5**, and **A5** → **indene** reactions, respectively. The **A22** → **A23** → **A5′** → **indene** sequence (pathway IV) within the 2−5 cyclization network (Figure 3) is also similar to pathway IX, except for the **A22** → **A23** bond scission, which exhibits a barrier almost 2 times lower than those for the analogous **A2** → **A3** and **A44** → **A45** reactions (this issue was already discussed in section 3.2.B). Similar to pathways I and IV, the alternative route **A45** → **A34** → **A12** → **indene** is hardly competitive with the major **A45** → **A12′** → **indene** route because the former involves an additional 3a−4 H shift **A34** → **A12** with a high barrier of 45.8 kcal/mol. Pathway IX was previously suggested and calculated at the B3LYP/6-31G** level by Wang et al.[6] (pathway R2 shown in Scheme 1). Our G3-calculated barriers for the reaction steps involved in this pathway agree within ~2−4 kcal/mol with their DFT results (see Table 1 for comparison). For the reaction energies, the differences are normally within 2−5 kcal/mol, except for the initial 3−5 cyclization **A0** → **A43**, where the discrepancy between the G3- and B3LYP-calculated parameters was found to be 9.2 kcal/mol.

Pathway X, **A45** → **A46** → **A36** → **A37**, leads to the formation of 1,7-dihydroazulene **A37** and is akin to the **A33** → **A35** → **A36** → **A37** (pathway VII), **A23** → **A25** → **A7′** → **A8** (pathway V), and **A3** → **A6** → **A7** → **A8** (pathway II) sequences within the 1−7 and 2−5 cyclization networks. All of these sequences have similar barriers and reaction energies for all involved rearrangements, except for the **A45** → **A46**, **A33** → **A35**, **A23** → **A25**, and **A3** → **A6** ring closures producing tricyclic intermediates. The **A45** → **A46** cyclization exhibits a 13.2 kcal/mol barrier and an exothermicity of 6.1 kcal/mol, which are close to those for **A3** → **A6** (13 and 3.1 kcal/mol, respectively) within pathway II. The **A33** → **A35** and **A23** → **A25** reactions have almost two times lower barriers (6.2 and 7.5 kcal/mol, respectively) and higher exothermicities (10.4 and 6.3 kcal/mol, respectively). Pathway X displays a significantly lower barrier for the initial **A45** → **A46** three-membered ring closure (13.2 kcal/mol) than that for the competing **A45** → **A12′** H shift (32.6 kcal/mol). This makes this pathway superior to pathway IX leading to indene. The same conclusion was made for the concurrent pathways IV and V considered for the 2−5 cyclization network. It is noteworthy that pathway X, alternatively to pathway IX, was not considered in the DFT study of Wang et al.[6]

Pathway XI, **A44** → **A47** → **A48** → **A18** → **A5** → **indene**, represents an analogue of pathway III, **A2** → **A9** → **A10** → **A11** → **A12** → **indene** (1−7 cyclization), with very similar energetics for the reaction steps involved; for both pathways, the barrier heights agree within 1−2 kcal/mol, and the reaction energies differ by 5−7 kcal/mol. In contrast to pathway III, we found a transition state for the direct conversion of **A44** to the tricyclic structure **A48**; in this process, the cleavage of a C−C bond in the CH_2 bridge occurs simultaneously with the transformation of the six-membered ring into two fused five-membered rings and one three-membered ring. In pathways III and VI, we were unable to locate transition states for similar direct isomerizations **A2** → **A10** and **A22** → **A27**, respectively. Although the direct **A44** → **A48** isomerization involves only one reaction step compared to the two-step **A44** → **A47** → **A48** mechanism, it exhibits a high barrier of 54.8 kcal/mol, whereas the consecutive **A44** → **A47** and **A47** → **A48** reactions demonstrate significantly lower barriers of 14.7 and 22.1 kcal/mol, respectively. This makes the direct **A44** → **A48** mechanism energetically unfavorable as compared to the stepwise **A44** → **A47** → **A48** process. The alternative **A48** → **A49** → **A50** → **A5′** → **indene** sequence (akin to the previously discussed **A10** → **A14** → **A12′** → **indene** route within the 1−7 cyclization network shown on Figure 2) involves two consecutive hydrogen-atom shifts **A48** → **A49** and **A49** → **A50** with relatively high barriers of 47.3 and 41.3 kcal/mol, respectively and, therefore, is not likely to compete with the more energetically favorable **A48** → **A18** → **A5** → **indene** route.

The last route within the 3−5 cyclization network, **A43** → **A51/A52** → **A40** → **A41/A42**, is denoted as pathway XII on Figure 4. Akin to pathway VIII **A20** → **A38/A39** → **A40** → **A41/A42** (2−5 cyclization), pathway XII leads to 1,8a-dihydroazulene **A41** and 1,3a-dihydroazulene **A42** via very similar intermediates and transition states with close energetic parameters. Since the initial **A20** → **A51** and **A20** → **A52** reactions demonstrate barriers of ~47 kcal/mol, close to the 44.6 kcal/mol barrier for the concurrent 7a−8 H migration **A43** → **A44**, one can expect a competition between pathway XII and the other routes within this network, as well as with the alternative 3a−8 H shift **A43** → **A2′** leading to the 1−7 cyclization network over a similar barrier of 45.4 kcal/mol.

3.3. Formation of Azulene and Naphthalene. The calculated 1−7, 2−5, and 3−5 cyclizations lead to indene and several azulene-like PAHs, **A8**, **A37**, **A41**, and **A42**, as the reaction products. These azulene precursors lie on the $C_{10}H_{10}$ PES, and in order to produce azulene, two consecutive H eliminations are required. Since the elimination of a hydrogen atom from a singlet species normally requires high energies, such a mechanism is energetically unfavorable. An alternative mechanism under combustion conditions can be a radical-promoted hydrogen abstraction reaction, which usually displays low barriers. The considered routes of azulene formation involving abstraction of hydrogen atoms from **A8**, **A37**, **A41**, and **A42** species are shown on Figure 5. In combustion flames where the concentra-

tion of free H radicals is expected to be high, these radicals may abstract H atoms linked to sp^3 carbons (CH_2 fragments) of **A8** and **A37**, producing 5-H-azulyl **A53** or 1-H-azulyl **A54** radicals. These reactions exhibit rather small barriers within 2−6 kcal/mol, which are significantly lower than those for the abstraction of H atoms linked to sp^2 carbons.[22] Interestingly, the H abstraction from the CH_2 fragment located on the five-membered ring (**A8** → **A53** and **A37** → **A53** reactions) requires barriers that are a factor of ∼2 higher as compared to the respective **A8** → **A54** and **A37** → **A54** abstractions from the CH_2 fragment located on the seven-membered ring. The abstractions of hydrogen atoms sitting at the 3a and 8a positions of **A41** and **A42** exhibit even lower barriers of 1.4 and 1 kcal/mol for **A41** → **A54** and **A37** → **A42**, respectively. The further eliminations of H atoms sitting at the 1 or 5 positions of **A54** or **A53**, respectively, lead to the formation of singlet azulene. Although the suggested bimolecular mechanisms display low barriers and are favorable energetically, they are kinetically favorable only if the concentration of free H or OH radicals required for H abstraction is significantly high. At low H radical concentrations, for instance, at low-temperature pyrolytic conditions, the abstraction mechanism of azulene formation can hardly be accomplished.

The H abstraction from **A8**, **A37**, **A41**, and **A42** leads to the $C_{10}H_9$ PES, and therefore, the **A53** and **A54** radicals on this surface can isomerize to naphthalene by, for example, the methylene walk pathway shown in Figure 5. This radical-promoted energetically favorable pathway was studied previously by Alder and co-workers[11] using a DFT method to explain the mechanism of azulene to naphthalene isomerization. Recently, it was revisited at the G3 level in our recent study of the 9-H-fulvalenyl radical rearrangements.[10] The mechanism involves several reaction steps in which the methylene group migrates from the six-membered to five-membered ring, and after ring expansion, the reaction sequence leads to the 1-H-naphthyl radical. According to our calculations, the methylene walk pathway exhibits reasonably low barriers for all reaction steps involved.[10] The **A53** radical is a more probable candidate to be involved in the methylene walk sequence; however, a competition with an alternative H elimination producing azulene should be taken into account. In contrast to **A53**, the **A54** isomer possesses the CH_2 fragment on the cyclopenta ring and therefore can be involved in methylene walk only after two consecutive (1−8a and 8a−8) H migrations, in which the hydrogen atom shifts from the cyclopenta to the seven-membered ring. In principle, **A53** and **A54** may participate not only in the methylene walk sequence but also in other rearrangements on the $C_{10}H_9$ PES, such as the spiran mechanism leading to naphthalene and so forth; see our previous publication[10] for detail. The H abstractions shown in Figure 5 serve as links connecting the $C_{10}H_{11}$ and $C_{10}H_9$ PESs, so that the products formed on the former may be involved (after H abstractions or eliminations) in isomerizations taking place on the latter and produce PAHs, such as naphthalene and fulvalene.

A question may arise about the feasibility of the methylene walk mechanism for some intermediates found on the $C_{10}H_{11}$ PES with structures similar to **A53** and **A54** radicals. In the calculated 1−7, 2−5, and 3−5 cyclization networks, the intermediates **A3**, **A23**, **A33**, and **A45** possess a methylene group linked to the six-membered ring and hence may be suitable for CH_2 group shifts akin to the methylene walk mechanism. The **A38**, **A39**, **A51**, and **A52** radicals may also be involved in similar rearrangements after scission of a C−C bond in the three-membered cycle fused to the six-membered ring. Therefore, one could expect that the methylene walk mechanism may take place on the $C_{10}H_{11}$ PES, leading to the formation of naphthalene core and, after elimination of three "extra" hydrogen atoms, to naphthalene. However, a closer inspection of these structures indicates that a methylene walk mechanism similar to that shown in Figure 5 has to include many more CH_2 migration steps and additional H migrations for the **A3**, **A23**, **A33**, **A45**, **A38**, **A39**, **A51**, and **A52** species. All of these structures have hydrogen atoms at the 3a or 7a positions, as well as a CH_2 fragment located on the cyclopenta ring; in other words, these structures have too many "extra" hydrogen atoms for the methylene walk sequence to be accomplished. These structural features impede the ability of straightforward migration of methylene from the six- to the five-membered ring. On the other hand, CH_2 migrations may lead to very unfavorable triradical structures, which make the methylene walk rearrangements unlikely as compared to the alternative pathways discussed above. For example, the 4−3a methylene shift in **A3** is prohibited because of the H atom present at the 3a position, but an alternative 4−5 migration leads to the formation of a triradical structure and is expected to have a very high barrier. Alternatively, the competing **A3** → **A5** → **indene** and **A3** → **A6** → **A7** → **A8** sequences exhibit low barriers and consist of only a small number of reaction steps.

3.4. Rate Constants and Product Yields. The calculated PES for rearrangements of the **A0** radical helps to elucidate energetically favorable pathways leading from **CPD** and **CPDyl** recombination products to indene and various precursors of azulene. However, in order to evaluate the contribution of each considered pathway to the formation of the reaction products, a calculation and thorough analysis of rate constants and relative product yields at temperatures relevant to combustion are required. Utilizing high-pressure-limit thermal rate constants for all unimolecular steps involved in the 1−7, 2−5, and 3−5 cyclization networks calculated using RRKM theory (collected in Table S2 of the Supporting Information), we computed the total product yields of indene, **A8**, **A37**, **A41**, and **A42** species as well as individual contributions of all considered pathways to the total product yields. It is worth noting that such calculations do not provide actual product yields in the real combustion and pyrolysis of hydrocarbon fuels and does not substitute extensive kinetic modeling of combustion systems, which is far more complicated. Nevertheless, it allows us to estimate the relative importance of each suggested pathway within the considered rearrangement networks.

The computed total product yields for rearrangements of the **A0** radical as well as contributions to these yields from various considered pathways are collected in Table 3. At all studied temperatures, indene is found to be the major reaction product (more than 50% of the total product yield) followed by 1,5-dihydroazulene **A8** (18−35%). 1,8a-Dihydroazulene **A41** and 1,3a-dihydroazulene **A42** are only minor products at typical combustion temperatures (less than 10% for **A41** and **A42** combined), whereas the production of 1,7-dihydroazulene **A37** is found to be negligible at all studied temperatures. At low and medium combustion temperatures (<2000 K), the overall production of azulene precursors, **A8**, **A37**, **A41**, and **A42**, is about a factor of 2 lower than that of indene, and only at very high temperatures (>2500 K) do their yields become close. The yields of indene are high both at low and medium temperatures; this explains why indene was found among the major reaction products in low-temperature **CPD** pyrolysis.[6] On the other hand, azulene or its derivatives were not reported as reaction products in ref 6, although our calculation shows significant yields of

TABLE 3: Calculated Product Yields (%) for Rearrangements of 8,9,10-Trihydrofulvalenyl Radical A0

	temperature, K										
product	500	700	1000	1200	1400	1500	1700	2000	2400	2800	3000
					Total Product Yields						
INDENE	64.9	63.6	64.8	65.3	65.2	64.9	64.0	61.7	58.4	55.2	53.7
A8	35.1	36.4	34.9	33.4	32.0	31.1	29.4	26.6	22.8	19.4	17.9
A37	0.0	0.0	0.0	0.01	0.04	0.06	0.12	0.24	0.42	0.57	0.63
A41	0.0	0.01	0.25	0.8	1.8	2.4	4.0	6.7	10.6	14.1	15.6
A42	0.0	0.0	0.12	0.43	1.0	1.5	2.5	4.6	7.7	10.7	12.1
A41 + A42	0.0	0.01	0.37	1.2	2.8	3.9	6.5	11.3	18.3	24.8	27.7
all azulene precursors **A8 + A37 + A41 + A42**	35.1	36.4	35.2	34.7	34.8	35.1	36.0	38.1	41.6	44.8	46.3
					Contributions to the Total Product Yields from the Considered Pathways						
INDENE (pathway I)	0.01	0.12	0.78	1.6	2.6	3.2	4.3	6.0	8.2	10.2	11.1
INDENE (pathway III)	62.9	57.8	52.4	49.0	45.6	43.9	40.5	35.6	29.6	24.4	22.2
INDENE **A17 → A19 → A5′ → IND**	0.0	0.0	0.0	0.0	0.0	0.0	0.0	0.0	0.0	0.0	0.01
INDENE **A17 → A18 → A5 → IND**	0.0	0.0	0.0	0.0	0.0	0.0	0.0	0.0	0.0	0.0	0.0
INDENE **A14 → A12′ → IND**											
A16 → A12′ → IND	0.0	0.0	0.0	0.01	0.03	0.06	0.14	0.35	0.79	1.3	1.6
INDENE (pathway IV)	2.0	5.7	11.5	14.4	16.4	17.1	17.9	18.0	17.0	15.6	14.8
INDENE (pathway VI)	0.0	0.0	0.0	0.0	0.0	0.0	0.0	0.0	0.0	0.02	0.03
INDENE (pathway VII)	0.0	0.0	0.0	0.0	0.0	0.0	0.0	0.0	0.0	0.01	0.02
INDENE (pathway IX)											
A45 → A12′ → IND	0.0	0.0	0.0	0.01	0.03	0.05	0.08	0.17	0.31	0.46	0.53
A45 → A34 → A12 → IND	0.0	0.0	0.02	0.06	0.14	0.18	0.29	0.47	0.71	0.9	0.98
INDENE (pathway XI)											
A48 → A18 → A5 → IND	0.0	0.01	0.09	0.22	0.42	0.53	0.8	1.2	1.8	2.2	2.4
A49 → A50 → A5′ → IND	0.0	0.0	0.0	0.0	0.0	0.0	0.0	0.01	0.03	0.07	0.1
A8 (pathway II)	0.0	0.05	0.39	0.85	1.5	1.8	2.5	3.4	4.3	4.8	4.9
A8 (pathway V)	35.1	36.3	34.5	32.6	30.5	29.3	26.9	23.2	18.6	14.7	13.1
A37 (pathway VII)	0.0	0.0	0.0	0.0	0.0	0.0	0.0	0.0	0.0	0.01	0.02
A37 (pathway X)	0.0	0.0	0.0	0.01	0.04	0.06	0.12	0.24	0.42	0.56	0.61
A41 + A42 (pathway VIII)	0.0	0.01	0.25	0.8	1.8	2.4	4.0	6.7	10.5	13.9	15.4
A41 + A42 (pathway XII)	0.0	0.0	0.12	0.43	1.0	1.5	2.6	4.7	7.8	10.9	12.3

1,5-dihydroazulene **A8** even at low temperatures corresponding to the **CPD** pyrolytic conditions. We suppose that **A8** is more likely to rearrange to naphthalene, another major product observed in **CPD** pyrolysis, after two consecutive H eliminations, for instance, by the methylene walk mechanism shown in Figure 5.

As follows from the calculated contributions to the total product yields, the pathway III in the 1−7 cyclization network is the major indene formation route, accounting for 50−80% of the total indene yield at 1000−2000 K. Pathway IV in the 2−5 cyclization network also gives significant contributions to the indene production, accounting for about 20−30% of the total indene yield at typical combustion temperatures. In contrast, pathway I, previously suggested by Wang et al.[6] as the major indene formation route in **CPD** pyrolysis, is found to be a minor indene formation channel, accounting for only 1−10% of the total indene yield within the 1000−2000 K range (<5% at typical combustion temperatures). Another route suggested in ref 6, pathway IX in the 3−5 cyclization network (R2 in Scheme 1), is computed to be negligible at temperatures relevant both to combustion and pyrolysis. The remaining indene formation routes (pathways VI, VII, XI, and **A17 → A19 → A5′ → IND**, **A17 → A18 → A5 → IND**, and **A14/A16 → A12′ → IND** sequences considered for alternative isomerizations of **A10** within the 1−7 cyclization network) exhibit zero or negligible contributions to the total indene yields and therefore can be excluded from consideration.

The highest contributions to the total product yields and that of indene are found for the 1−7 cyclization network, which includes pathway III. This is not surprising because, as discussed in section 3.2, the **A0 → A1** cyclization is significantly more favorable energetically and kinetically than the competing **A0 → A20** and **A0 → A43** cyclizations. Pathway III was also found to be superior over the other routes within the 1−7 cyclization network, that is, pathways I and II. Both of these pathways start from the **A2 → A3** C−C bond scission, which is considerably less favorable than the concurrent **A2 → A9** isomerization (see section 3.2.A). A comparison of the individual rate constants collected in Table 2 shows that the latter reaction has rate constants several orders of magnitude higher than those of the

former within the 1000−2000 K temperature range (e.g., the k(**A2** → **A9**)/k(**A2** → **A3**) ratio is 1716 at 1500 K). Because the **A2** → **A9** reaction is much faster than its competitors and further rearrangements of **A9** to indene involve reaction steps with low barriers and therefore with high rate constants, pathway III is more kinetically favorable than the concurrent pathways I and II. Another competing **A2** → **A43′** isomerization has even lower rate constants (by ∼1−2 orders of magnitude lower than those for **A2** → **A3**) and is thus insignificant. The production of indene by alternative routes within pathway III originating from **A10** → **A13** and **A10** → **A17** isomerizations was found to be negligible, as follows from the individual product yields for the **A17** → **A19** → **A5′** → **IND**, **A17** → **A18** → **A5** → **IND**, **A14** → **A12′** → **IND**, and **A16** → **A12′** → **IND** sequences. This result can be explained by comparing the rate constants for the **A10** → **A11**, **A10** → **A13**, and **A10** → **A17** steps presented in Table 2. At all considered temperatures, the **A10** → **A11** H-migration reaction exhibits rate constants several orders of magnitude higher than those for **A10** → **A13** and especially **A10** → **A17**; the latter goes through a high barrier of 72.4 kcal/mol. At a typical combustion temperature of 1500 K, the k(**A10** → **A11**)/k(**A10** → **A13**) and k(**A10** → **A11**)/k(**A10** → **A17**) ratios are calculated to be 382 and 7.5×10^6, respectively.

The contributions of pathway IV (2−5 cyclization network) to the indene production were found to be lower than those of pathway III, but they are still significant at typical combustion temperatures, giving 20−30% of the total indene yield at 1000−2000 K. This may look surprising considering that the **A0** → **A1** reaction is significantly faster and exhibits much higher equilibrium constants (see Table 2) within this temperatures range than **A0** → **A20**, which starts the 2−5 cyclization network. However, within the 1000−2000 K range, further isomerization of **A1**, via the 7a−1 H shift **A1** → **A2** with a high barrier of 50.6 kcal/mol, has rate constants 2−6 orders of magnitude lower and equilibrium constants 3−7 orders of magnitude lower than the respective values for the 8−1 H shift **A20** → **A21**. This means that the **A1** → **A2** step is slow (rate-limiting) and the equilibrium is shifted toward **A1** ($K_{eq} < 1$), in contrast to the fast **A20** → **A21** reaction, where the equilibrium is shifted toward the product **A21** ($K_{eq} > 1$). In such a case, one has to consider the competition between the **A0** → **A1** → **A2** and **A0** → **A20** → **A21** sequences, taking into account both rate and equilibrium constants for the steps involved. The **A0** → **A1** reaction is favored over the competing **A0** → **A20** step, but the subsequent **A1** → **A2** H shift inhibits the production of **A2**. On the other hand, the fast **A20** → **A21** isomerization partially compensates for the slow initial **A0** → **A20** process promoting production of indene via pathway IV. Although pathway IV significantly contributes to the indene formation, it is not the major pathway within the 2−5 cyclization network. Alternatively, the major route in this network is pathway V, leading to the production of 1,5-dihydroazulene **A8** and accounting for 70−100% of the total yield of **A8**, depending on temperature. This result follows from the calculated energetics and rate constants for both pathways. Indeed, pathway V exhibits significantly lower barriers and higher rate constants for the critical **A23** → **A25** and **A25** → **A7′** reaction steps, as compared to the respective **A23** → **A4′** and **A4′** → **A5′** reactions in pathway IV. For instance, at 1000−2000 K, the k(**A23** → **A25**)/k(**A23** → **A4**) ratios are within 6.6×10^4−75 and the k(**A25** → **A7′**)/k(**A4′** → **A5′**) ratios are within 7.6×10^4−250 (see Table 2). This makes pathway V more kinetically favorable than the competing pathway IV. In addition, in contrast to similar pathway I, the direct **A23** → **A5′** H-atom migration is impossible in pathway IV. As a result, this process has to involve two consecutive **A23** → **A4′** and **A4′** → **A5′** H shifts with relatively high barriers, which inhibit the formation of indene.

The indene production via pathway VI is found to be negligible at all studied temperatures, in contrast to similar pathway III (1−7 cyclization network), which is the major pathway among all rearrangements of **A0**. Although the initial **A22** → **A26** reaction is slightly faster than the competing **A22** → **A23** step at typical combustion temperatures, the further rearrangements of **A26** exhibit higher barriers and slower rate constants as compared to those for the reactions involved in pathways IV and V.

The indene production in pathways IX and XI of the 3−5 cyclization network is also insignificant, as is the production of 1,7-dihydroazulene **A37** via pathway X. Although the initial **A0** → **A43** reaction, which starts rearrangements in the 3−5 cyclization network, demonstrates energetics and reaction rates similar to those for **A0** → **A20**, which initiates the 2−5 cyclization network, the subsequent **A43** → **A44** isomerization exhibits a high barrier of ∼45 kcal/mol and therefore significantly lower reaction rates compared to those for the respective **A20** → **A21** reaction (see Table 2). In other words, in contrast to the **A0** → **A20** → **A21** reaction sequence, **A0** → **A43** → **A44** involves two consecutive steps with low rate constants, which makes the rearrangements within the 3−5 cyclization network kinetically unfavorable. The only exception is pathway XII, which does contribute to the formation of **A41** + **A42** at high combustion temperatures.

1,5-Dihydroazulene **A8** can be produced by two routes, pathways II and V of the 1−7 and 2−5 cyclization networks, respectively. Pathway V is the major **A8** formation route, accounting for about 90% of the total **A8** yield within 1000−2000 K, whereas pathway II gives only a minor contribution, 1−13% within the same temperature range. Pathway V is superior over the other competing routes IV and VI within the 2−5 cyclization network because it shows lower barriers and higher rate constants (see Table 2) for the steps involved. In contrast to pathway V, the contribution of pathway II, which demonstrates similar energetics and rate constants, is not as significant because the latter one loses competition to more favorable pathway III. As was discussed above, the critical **A2** → **A3** and **A2** → **A9** steps control the competition between the pathways within the 1−7 cyclization network, and the latter, which starts pathway III, is significantly faster than the former at typical combustion temperatures. Although the relative contributions of pathway II to the **A8** production are found to be minor, they are not insignificant, especially at higher combustion temperatures. Hence, we suggest keeping this route under radar in further kinetic modeling simulations.

The production of another azulene precursor, 1,7-dihydroazulene **A37**, was found to be negligible at all studied temperatures. This is not surprising because the only two routes, which lead to this product, for example, pathways VII and X within the 2−5 and 3−5 cyclization networks, respectively, exhibit considerably higher barrier and lower rate constants for the critical reactions as compared to the other competing pathways within these networks. Indeed, pathway VII involves two initial steps **A20** → **A31** and **A31** → **A32** with very high barriers of about 70 kcal/mol, and, as a consequence, these steps exhibit low rates. Meanwhile, the competing **A20** → **A21** and **A21** → **A22** steps, which start pathways V, VI, and VII, have rate constants several orders of magnitude higher (see Table 2). The other two competing reactions **A20** → **A38** and **A20** → **A39**,

which start pathway VIII and eventually lead to **A41** and **A42**, also exhibit higher rates. Pathway X of the 3−5 cyclization network leading to the formation of **A37** is also hardly competitive with the other routes within this network because it can be accomplished only after two consecutive isomerizations **A43** → **A44** and **A44** → **A45** with barriers of about 45 kcal/mol. These two steps are unfavorable when compared to the respective competing reactions in pathways XI and XII.

The last two products found in rearrangements of the **A0** radical, 1,8a-dihydroazulene **A41** and 1,3a-dihydroazulene **A42**, can be formed by pathways VIII and XII of the 2−5 and 3−5 cyclization networks, respectively. Both pathways demonstrate very similar energetics and rate constants and similar contributions to the total **A41** + **A42** product yields, with pathway VIII giving a slightly higher input. At temperatures below 1500 K, the production of **A41** and **A42** is insignificant (less than 5%); however, at higher combustion temperatures, it becomes noticeable (>10% at T > 2000 K). Pathway XII is found to be the major pathway within the 3−5 cyclization network; it shows considerably higher contributions to the total product yields as compared to the other pathways IX, X, and XI in this network.

3.5. Suggested Mechanism of PAH Growth Involving Reactions of CPD and CPDyl. Using the results of our G3 calculations of the PES for rearrangements of the 8,9,10-trihydrofulvalenyl radical **A0** as well as the computed relative product yields, we constructed the concluding reaction scheme including only the pathways with noticeable contributions to the formation of the reaction products, indene, **A8**, **A41**, and **A42**. We also combined the current results with the previously calculated mechanism for rearrangements of the 9-H-fulvalenyl radical (**S1**), which take place on the $C_{10}H_9$ PES;[10] this mechanism was also thoroughly investigated at the same G3 level with calculations of relative product yields. The summary of all studied mechanisms on both PESs is shown in Figure 6, along with G3-computed barrier heights, heats of reactions, and energies relative to **A0** (for the $C_{10}H_{11}$ PES) and **S1** (for $C_{10}H_9$ PES, marked with asterisks). The mechanism on the $C_{10}H_{11}$ part of the PES only retains pathways I−V, VIII, and XII, whereas the other routes are excluded due to their negligible contributions to the product yields. Pathways III and V give the highest contributions (more than 50% at typical combustion temperatures) to the production of indene and 1,5-dihydroazulene **A8**, respectively, but pathways I, II, IV, VIII, and XII represent only minor reaction channels. It should be noted that for pathways I−V, we have not included similar pathways with optical isomers (see Figures 2 and 3), which have the same energetics and rate constants as those of the original pathways. For the purpose of kinetic simulation, rate constants of all reaction steps in I−V should be simply multiplied by a factor of 2 to take into account the existence of the analogous routes via optical isomers.

The $C_{10}H_9$ part of the PES leads to the production of naphthalene, azulene, and fulvalene and includes the well-known spiran mechanism, as well as the C−C bond scission and methylene-walk pathways.[6,10,11,23] These reaction sequences and their relative contributions to the total product yields at combustion temperatures were analyzed in detail in our previous study.[10] We suppose that the overall mechanism shown in Figure 6 represents, at this time, the most complete description of the processes taking place on the $C_{10}H_9$ and $C_{10}H_{11}$ PESs and originated from the reactions involving highly abundant **CPD** and **CPDyl** species. This final mechanism includes several previously suggested pathways thoroughly revisited by our G3 calculations and introduces a number of new routes, which were shown to be significant contributors to the PAH formation. Although there is always a possibility to miss a certain pathway in such a complicated mechanism, we believe that the suggested scheme is complete enough for the purpose of kinetic modeling and involves all major channels leading from reactions of **CPD** and **CPDyl** to indene, naphthalene, azulene, and fulvalene through rearrangements on the $C_{10}H_9$ and $C_{10}H_{11}$ PESs. The only missing piece of the puzzle is the rearrangements on the singlet $C_{10}H_{10}$ PES starting from the recombination product of two **CPDyl** radicals, 9,10-dihydrofulvalene **S0**. The calculations of the $C_{10}H_{10}$ PES is ongoing in our group. The final mechanism shown in Figure 6 can be incorporated into the existing schemes for kinetic modeling of PAH growth both in combustion and pyrolysis utilizing the calculated rate constants for all reaction steps involved. Under the conditions where the high-pressure limit is adequate, this should improve the prediction of concentration profiles and relative product yields of indene and other PAH species considered here. Otherwise, when temperature- and pressure-dependent rate constants $k(T,p)$ are required, they can be obtained by solving time-dependent, multiple-well master equations (ME), and the present results on the PES and molecular properties will provide raw data for such RRKM/ME calculations.

4. Conclusions

In the present study, we performed rigorous Gaussian-3-type investigations of various reaction pathways taking place on the $C_{10}H_{11}$ PES originating from the recombination of two **CPDyl** radicals and intermolecular addition of **CPDyl** to **CDP**. The present calculations of rearrangements of the 8,9,10-trihydrofulvalenyl radical **A0** are complementary to our previous G3 study of rearrangements of the 9-H-fulvalenyl radical **S1** on the $C_{10}H_9$ potential, and the combined results for the two PESs represent, at this time, the most complete picture of the radical-promoted reaction mechanisms leading from c-C_5 species to a variety of PAHs abundant in combustion flames, including indene, naphthalene, azulene, and fulvalene. In total, 12 reaction pathways for rearrangements of **A0** were considered and mapped out at the G3 level, which was followed by statistical theory calculations of high-pressure-limit thermal rate constants and relative product yields within the 300−3000 K temperature range. At T = 1000−2000 K, relevant to combustion, indene was found to be the major reaction product (>50%) followed by 1,5-dihydroazulene **A8** (25−35%). The production of the other considered azulene precursors was found to be either minor (1,8a-dihydroazulene **A41** and 1,3a-dihydroazulene **A42**) or negligible (1,7-dihydroazulene **A37**). The calculation of the relative contributions of all 12 considered pathways to the total product yields allowed us to select only seven pathways (Figure 6) for the final kinetic scheme, which is suggested for future kinetic simulations of PAH formation in real combustion systems. The calculated high indene product yields are consistent with experimental observations of the low-temperature pyrolysis of cyclopentadiene,[5,6] where indene and naphthalene were found as the major reaction products. The mechanisms of indene formation starting from the **CPD** + **CPDyl** reaction previously suggested and studied by Wang et al.[6] using a DFT method to explain high indene yields in **CPD** pyrolysis were revisited in the present study (pathways I and IX). Although we found a good agreement of the B3LYP-calculated barriers and heats of reactions computed by Wang et al. with our G3 results, the contributions of pathways I and IX to the indene production were found to be either small (pathway I) or even insignificant (pathway IX) at typical combustion temperatures. According

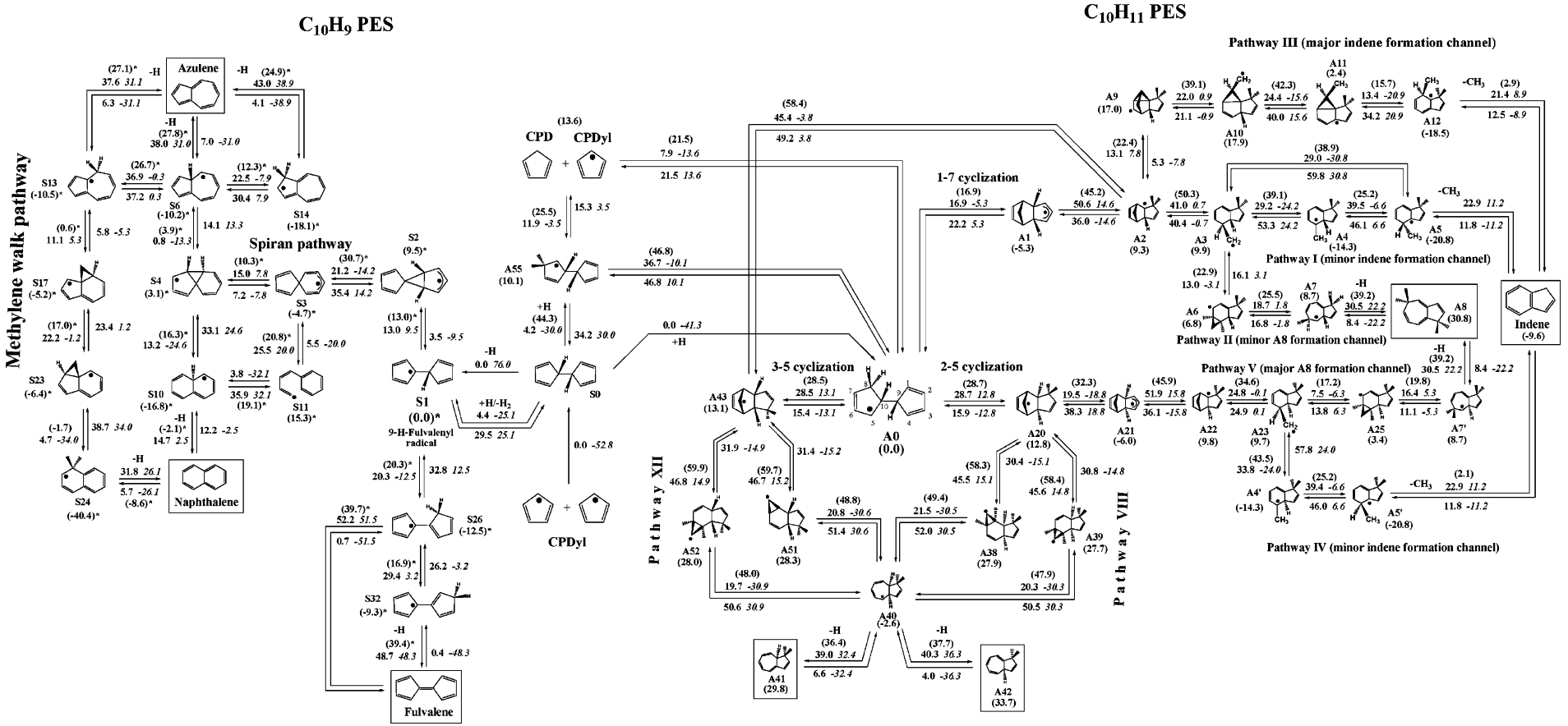

Figure 6. Summary of the most important pathways on the $C_{10}H_9$ and $C_{10}H_{11}$ PESs originating from reactions of **CPD** and **CPDyl**. The numbers along the arrows show G3(MP2,CC)//B3LYP-computed barrier heights and heats of reactions (in italics) in kcal/mol. The numbers shown in parentheses represent the energies (kcal/mol) relative to **A0** and **S1** (denoted with asterisks).

to our calculations, the most energetically and kinetically favorable indene formation mechanism is pathway III, which was not suggested previously, as were not various pathways leading to azulene precursors **A8**, **A41**, and **A42**. Since our G3-computed PESs should be of high accuracy, we expect the resulting rate constants to be also rather accurate for the conditions where the high-pressure limit is adequate. Otherwise, the PES information for all reaction steps in the considered mechanisms represent a suitable set of the raw data for the future RRKM/ME calculations of temperature- and pressure-dependent rate constants, which can be then included in the existing kinetic schemes for kinetic simulations of PAH formation in real flame combustion.

Acknowledgment. This work is funded by the Chemical Sciences, Geosciences and Biosciences Division, Office of Basic Energy Sciences, Office of Sciences of U.S. Department of Energy (Grant No. DE-FG02-04ER15570).

Supporting Information Available: Calculated total energies at the B3LYP/6-311G** level, zero-point energy corrections, vibrational frequencies, moments of inertia, rotational constants, and optimized Cartesian coordinates of all species involved in the studied mechanisms (Table S1); rate constants of all studied reactions within the 300−3000 K temperature range (Table S2). This material is available free of charge via the Internet at http://pubs.acs.org.

References and Notes

(1) Marinov, N. M.; Pitz, W. J.; Westbrook, C. K.; Vincitore, A. M.; Castaldi, M. J.; Senkan, S. M.; Melius, C. F. *Combust. Flame* **1998**, *114*, 192.

(2) Castaldi, M. J.; Marinov, N. M.; Melius, C. F.; Huang, J.; Senkan, S. M.; Pitz, W. J.; Westbrook, C. K. *Proc. Int. Symp. Combust.* **1996**, *26*, 693.

(3) Marinov, N. M.; Pitz, W. J.; Westbrook, C. K.; Castaldi, M. J.; Senkan, S. M. *Combust. Sci. Technol.* **1996**, *116*, 211.

(4) Granata, S.; Faravelli, T.; Ranzi, E.; Olten, N.; Senkan, S. *Combust. Flame* **2002**, *131*, 273.

(5) Lu, M.; Mulholland, J. A. *Chemosphere* **2004**, *55*, 605.

(6) Wang, D.; Violi, A.; Kim, D. H.; Mullholland, J. A. *J. Phys. Chem. A* **2006**, *110*, 4719.

(7) Fascella, S.; Cavallotti, C.; Rota, R.; Carra, S. *J. Phys. Chem. A* **2004**, *108*, 3829.

(8) Kislov, V. V.; Mebel, A. M. *J. Phys. Chem. A* **2007**, *111*, 3922.

(9) Richter, H.; Howard, J. B. *Prog. Energy Combust. Sci.* **2000**, *26*, 565.

(10) Kislov, V. V.; Mebel, A. M. *J. Phys. Chem. A* **2007**, *111*, 9532.

(11) Alder, R. W.; East, S. P.; Harvey, J. N.; Oakley, M. T. *J. Am. Chem. Soc.* **2003**, *125*, 5375.

(12) (a) Becke, A. D. *J. Chem. Phys.* **1992**, *96*, 2155. (b) Becke, A. D. *J. Chem. Phys.* **1992**, *97*, 9173. (c) Becke, A. D. *J. Chem. Phys.* **1993**, *98*, 5648. (d) Lee, C.; Yang, W.; Parr, R. G. *Phys. Rev. B* **1988**, *37*, 785.

(13) (a) Baboul, A. G.; Curtiss, L. A.; Redfern, P. C.; Raghavachari, K. *J. Chem. Phys.* **1999**, *110*, 7650. (b) Curtiss, L. A.; Raghavachari, K.; Redfern, P. C.; Baboul, A. G.; Pople, J. A. *Chem. Phys. Lett.* **1999**, *314*, 101.

(14) Curtiss, L. A.; Raghavachari, K.; Redfern, P. C.; Rassolov, V.; Pople, J. A. *J. Chem. Phys.* **1998**, *109*, 7764.

(15) Mebel, A. M.; Kislov, V. V. *J. Phys. Chem. A* **2005**, *109*, 6993.

(16) Frisch, M. J.; Trucks, G. W.; Schlegel, H. B.; Scuseria, G. E.; Robb, M. A.; Cheeseman, J. R.; Zakrzewski, V. G.; Montgomery, J. A., Jr.; Stratmann, R. E.; Burant, J. C.; Dapprich, S.; Millam, J. M.; Daniels, A. D.; Kudin, K. N.; Strain, M. C.; Farkas, O.; Tomasi, J.; Barone, V.; Cossi, M.; Cammi, R.; Mennucci, B.; Pomelli, C.; Adamo, C.; Clifford, S.; Ochterski, J.; Petersson, G. A.; Ayala, P. Y.; Cui, Q.; Morokuma, K.; Malick, D. K.; Rabuck, A. D.; Raghavachari, K.; Foresman, J. B.; Cioslowski, J.; Ortiz, J. V.; Stefanov, B. B.; Liu, G.; Liashenko, A.; Piskorz, P.; Komaromi, I.; Gomperts, R.; Martin, R. L.; Fox, D. J.; Keith, T.; Al-Laham, M. A.; Peng, C. Y.; Nanayakkara, A.; Gonzalez, C.; Challacombe, M.; Gill, P. M. W.; Johnson, B. G.; Chen, W.; Wong, M. W.; Andres, J. L.; Head-Gordon, M.; Replogle, E. S.; Pople, J. A. *Gaussian 98*, revision A.11; Gaussian, Inc.: Pittsburgh, PA, 2001.

(17) Amos, R. D.; Bernhardsson, A.; Berning, A.; Celani, P.; Cooper, D. L.; Deegan, M. J. O.; Dobbyn, A. J.; Eckert, F.; Hampel, C.; Hetzer, G.; Knowles, P. J.; Korona, T.; Lindh, R.; Lloyd, A. W.; McNicholas, S. J.; Manby, F. R.; Meyer, W.; Mura, M. E.; Nicklass, A.; Palmieri, P.; Pitzer, R.; Rauhut, G.; Schutz, M.; Schumann, U.; Stoll, H.; Stone, A. J.; Tarroni, R.; Thorsteinsson, T.; Werner, H.-J. *MOLPRO, a Package of Ab Initio Programs*, version 2002.1; designed by Werner, H.-J., Knowles, P. J..

(18) Steinfield, J.; Francisco, J.; Hase, W. *Chemical Kinetics and Dynamics*; Prentice Hall: Englewood Cliffs, NJ, 1989.

(19) Eyring, H.; Lin, S. H.; Lin, S. M. *Basic Chemical Kinetics*; Wiley: New York, 1980.

(20) Robinson, P. J.; Holbrook, K. A. *Unimolecular Reactions*, Wiley: New York, 1972.

(21) Glasstone, S.; Laidler, K. J.; Eyring, H. *The Theory of Rate Processes*; McGraw-Hill: New York, 1941.

(22) Kislov, V. V.; Islamova, N. I.; Kolker, A. M.; Lin, S. H.; Mebel, A. M. *J. Chem. Theory Comput.* **2005**, *1*, 908.

(23) Melius, C. F.; Colvin, M. E.; Marinov, N. M.; Pitz, W. J.; Senkan, S. M. *Proc. Int. Symp. Combust.* **1996**, *26*, 685.